CONF-9010197--2

EGG-M-90444

COMBUSTION SPACE MODELLING OF OXY-FUEL FIRED GLASS MELTER

Wolfgang Richter
Consultant
Irvine, California 92714

EGG-M--90444

DE91 001886

Hisashi Kobayashi
Union Carbide Industrial Gases, Inc., Linde Division
Tarrytown, New York 10561

ABSTRACT

A three-dimensional heat transfer code based on the zonal method was applied to evaluate the oxygen-fuel firing of a cross-fired regenerative glass melter. A furnace end section which includes the bridge wall and a pair of the regenerator ports was modelled in detail for a base air case and several oxy-fuel firing cases. The firing rates of two oxy-fuel burners that matched the heat flux distribution of the base air case were determined. The effects of the height and angle of the oxy-fuel burners on the temperature and heat flux distributions were predicted to evaluate the optimum burner placement of the oxy-fuel burners. The main conclusions of the simulation are that; (1) in spite of the small flame diameters, the high momentum low flame temperature oxy-fuel burners can create temperature and heat flux distributions equivalent to those of the base air case with a wide flame and (2) both lower burner elevation and angling of the oxy-fuel burners toward the glass surface tend to increase heat transfer to glass surface and reduce the peak refractory temperatures.

INTRODUCTION

Oxygen-fuel firing of glass melters is gaining increasing industry acceptance as a viable way to reduce NOx, particulates and other toxic emissions and to improve energy efficiency. Small specialty glass tanks have been converted to oxygen firing and operating commercially for several years (Ref. 1). A 110 TPD unit melter was converted to oxygen firing about a year ago (Ref. 2). Union Carbide Industrial Gases (UCIG), Inc. has recently conducted successful oxy-fuel firing programs in large tanks for glass bottles and fibers. Since the combustion and heat transfer conditions with oxy-fuel firing can be substantially different from those with the conventional air firing, retrofitting of existing air fired furnaces with oxy-fuel burners requires a careful selection of the type and number of oxy-fuel burners and their proper placement on the glass tank walls. At present these burner decisions are made based on (1) experiences in other industrial furnaces, (2) experimental data on flame characteristics of small scale burners in test furnaces and (3) theoretical heat transfer considerations. Very conservative approaches are generally taken in converting existing furnaces and designing new furnaces for oxy-fuel firing to avoid costly commercial mistakes.

The optimum furnace design with oxy-fuel firing is likely to be different from the existing furnaces designs for air firing due to a sharp reduction in the flue gas volume and to the heat transfer rate increase possible with oxy-fuel firing. Numerical modelling of the combustion space of glass furnaces offers potential to optimize the furnace design and burner placement for oxy-fuel firing. Although numerical simulation has been used for many years to understand the mechanism of glass melting and for commercial design of glass furnaces, simplified heat transfer models were often used for the combustion space as the focus of modelling was the analysis of glass flow patterns (Ref. 3). In particular, most of these simplified combustion space heat transfer models, do not account for the effects of flame position and characteristics on glass bath heat transfer.

On the other side, advances in numerical methods and computer speed and capacities, have led to the development of complex models, which directly couple comprehensive 3-D finite-difference combustion space analysis, with 3-D melter analysis (Refs. 4,5). However, these latter models, while attractive in the straightforwardness of their approach, require still an enormous effort in time to set up and to validate, and in computational and financial resources to run.

Therefore, the current analysis was based on a approach which is complex enough to allow to study the impact of local flame radiation on heat transfer to the glass, but which avoids the complexity of the comprehensive models by using simplified boundary conditions at the glass surface and by decoupling the combustion space gas flow analysis, as well.

APPROACH

The current approach uses a 3-D heat transfer and combustion zone model, which allows accurate assessment of local radiative heat transfer between gas heat sources, furnace gas volume, refractory walls and heat sinks. Furnace flow and flame heat release pattern are semi-empirically prescribed. However, flame heat release patterns are based on measurements in pilot-scale furnaces and actual flame observations. Thermal boundary conditions at the glass surface are simplified either by assigning effective temperatures and emissivities, or by use of a simple heat conduction model into the glass bath. Use of these simplified boundary conditions is justified by the fact that one of the goals of the current study is to identify O2-Burner configurations which generate similar net heat flux distributions as does conventional air firing.

A further simplification was introduced by considering only a section of a cross-fired glass furnace. In the current project only the end-section of such a furnace was modelled. This allowed to use computational grids small enough that the computer code of the model could be executed on PC's. The model developed for above approach is described in detail in the following sections.

3-D Zone Model

As already mentioned, the present study is based on a 3-D heat transfer and combustion zone model (Ref. 6). This model has successfully been applied in the past for thermal performances studies of a variety of boiler, industrial and pilot-scale furnaces (Ref. 7) including furnaces almost completely insulated by refractory walls like a glass furnace. The model is especially suitable for the latter furnaces, since emphasis is laid on accurate treatment of multi-directional radiative exchange, which is by far the dominant mode of heat transfer in these high temperature furnaces.

In zone-type models such as the current one, the combustion space is sub-divided by a net of well-stirred volume zones, and by a net of corresponding boundary zones. Average zone temperatures are obtained of total energy balances set up for each zone. The heat balance for a volume zone is formulated by Eq. (1) :

$$Q_r + Q_s + Q_d - Q_{ch} = 0 \quad , \tag{1}$$

where Q_r and Q_s are the net heat fluxes over the zone boundaries by radiation and advection, respectively. Q_d, which is small in high temperature furnaces, represents the convective transport through a wall boundary layer from a near wall volume zone to a adjacent surface zone. Q_{ch}, finally is the net heat release in the volume zone due to flame reactions obtained from species balances solved in addition to the volume zone heat balances.

Contrary to the more expensive finite-difference combustor models, the advective mass flow rates necessary to calculate the terms Q_s in Eq. (1) are not obtained from a simultaneous solution of momentum balances, but are rather input into the zone model, thus allowing to spend available computational resources for a more accurate simulation of radiative exchange.

The multi-directional transport of radiative energy between all wall and surface zones (i.e. term Q_r in Eq. (1)) is calculated with the semistochastic method (Ref. 6). This method which is derived from Monte-Carlo calculation techniques is illustrated in Fig. 1. Q_r is expressed by Eq. (2) :

$$Q_r = 4\ V\ \Sigma^4_{n=1}\ a_n K_n\ \sigma T_g^4 - \Sigma^4_{n=1}\ \Sigma_{beam}\ Q_{beam,a} \qquad (2)$$

Eq. (3) implies that the radiative properties of the combustion products are approximated with a so-called 'Weighted-Grey-Gas Approach' (Ref. 8) with n=4 grey ranges. a_n is the weighing factor and K_n is the grey absorption co-efficient assigned to the n th range.

The radiation model works as follows. The emissive power of all grey ranges (1 st term of Eq. (2)) of a volume zone (surface zones are treated in analogy) is distributed among a finite number of beams. The beams are emitted over the whole view angle and traced through the arrangement of volume zones until they impinge on wall. The beam gradually loose energy through absorption. The amount of energy $Q_{beam,a}$ absorbed from a beam by a volume zone is expressed by :

$$Q_{beam,a} = Q_{beam,in}\ [1-\exp(-K_n\ ds)] \qquad (3)$$

$Q_{beam,in}$ is the energy flux of a beam incident on the volume zone and ds is the path length of the beam cut out by this zone. The energy amounts $Q_{beam,a}$ absorbed from all beams passing a zone are accumulated. The radiative sub-balance according to Eq. (2) is calculated for each iteration cycle necessary to solve the total energy balance (1).

Since in the current study wall surfaces are treated as grey, diffuse radiators and reflectors, reflected energy amounts from beams incident on a wall are accumulated at the corresponding surface zones, and added to surface emission in the next iteration step. Combined wall emission and reflection is then treated in analogy of volume emission described above, however taking the cosine law into account.

The current semistochastic method is distinguished from pure Monte-Carlo methods by the fact, that some events in the history of a beam are deterministically influenced rather than based solely on random numbers (see Ref. 6).

The zone model considers, besides radiation from wall zones, radiation from gaseous species CO2 and H2O and from soot particles. Zonal concentration of these species are calculated from the combustion model described further below. Weighing factors and specific absorption coefficients of the gaseous species utilized for the 'Weighted-Grey-Gases-Approach' are taken from Ref. 8. The specific absorption coefficients for soot are prescribed according to an approach suggested in Ref. 9.

Furnace Flow Distribution and Heat Release Pattern

Furnace Flow Field

Besides the radiation terms, the total energy balance of each volume zone includes contributions from convective transport and from heat release due the flame reactions. As mentioned above, the advective transport of sensible heat is based on predetermined zonal mass flux distributions. There are several means to obtain such distributions ranging from simple engineering guesses to sophisticated 3-D fluid dynamics calculations. In the present study, suitable furnace flow distributions were determined from a mixed-type approach, combining enclosed jet theory, educated guesses and computer routines for continuity considerations and for direct graphical display of mass flux density vectors.

The jet theory was in particular applied to estimate the flow for the O_2 firing configuration. It was assumed that the forward flows of the high momentum O_2-jets which fired from opposite furnace sides in a staggered manner, were not interacting. The flow fields associated with each burner were constructed as follows.

The multi-jet outlet of an O_2 burner was replaced by an equivalent nozzle diameter taking flame expansion into account. Forward flow profiles and local entrainment rates were calculated with the assumption that the jet entrains fluid halfway the distance between jet origin and impingement of the jet envelope at surrounding walls. The backflow necessary to support the entrainment rates was empirically distributed over the furnace with help of profile factors.

In a final step, the flow fields derived for the individual burners were arithmetically superimposed. Also superimposed are pairs of turbulent mass flux vectors with prescribed strength, in order to simulate large scale turbulent exchange over zone boundaries. The simple approach described above is currently validated by 3-D fluid dynamics modeling. Entrainment rates of the O_2-flames were also validated with results of comprehensive 2-D modeling previously carried out for pilot-scale O_2-burner trials (Ref. 10).

Combustion Model

The calculation of zonal heat release is based on the furnace flow obtained from above model and on an empirical function, which accounts for the mixing controlled progress of burn-out. In this model, the gaseous fuel is represented by fuel lumps, which follow the turbulent flow. The lumps are tracked within the zone arrangement. The lifetime of individual lumps is statistically

calculated with help of weighted random numbers in such a way that the unburnt matter of a large assembly gas fuel lumps of same origin is an exponential function of residence time t :

$$Q_{unb}/Q_{unb,o} = \exp\left[-(1/c_b)\,(t/t_b)^m\right] \qquad (4)$$

$Q_{unb,o}$ is the sum of chemical heat of all gaseous fuel lumps originating from the same burner inlet zone, and Q_{unb} is the corresponding amount after time t. Accumulation of chemical heat from all fuel lumps reacted in a volume zone yields the chemical source term Q_{ch} needed for the total energy balance (Eq. 1). By using the value 0.1448 for the constant c_b, t_b can be identified as the time needed to achieve (at least on average) burn-out down to 99.9%.

In the current study, the heat release distribution in the air flames was calculated using t_b = 0.75 s and m = 2. The value for t_b was chosen so, that 99.9% burn-out was achieved just at the flue gas port. Thus the observed flame length was matched.

The time constant tb for the O_2 flames was chosen so that the length of the O_2 flames observed in pilot scale experiments was matched. Fig. 2 shows measured axial values of unburnt fuel and of O_2-concentration dependent on distance from the O_2 burner normalized with an equivalent nozzle diameter d_{eq}. The distance Z/d_{eq} = 121.2 represents the width of the furnace investigated in the current study. Also plotted into Fig. 2 are burn-out distributions based on Eq. 4 and used in the model. The curves denoted by A5 represent an O_2 flame with a load 3.71 higher than the flame represented by curves A6 (see also below). Both sets of curves were obtained for m = 3. For flame A5, t_b = 0.045 s was utilized and for the lower load flame, t_b = 0.167 s, i.e. the ratio for t_b of both flames was assumed to be proportional to their load ratio.

The heat release model described above is coupled with species transport equations which allow to calculate zonal concentrations of major combustion products and O_2 needed to compute specific heats. The zonal concentrations of CO_2 and H_2O are also used to calculate zonal absorption coefficients K_n as required by Eq. (2). The current radiation model requires additionally estimation of flame soot concentrations. Whereas the O_2 flames are soot free, luminous radiation plays a certain role in air flames. The natural gas/air flames considered in this study were very sooty. In order to calculate soot absorption coefficients in these flames, it was assumed that flame soot is present in a zone in proportion to unburnt fuel calculated with above combustion model for the same zone. An empirical value was used for the constant of proportionality.

Thermal Boundary Conditions

Prescription of thermal boundary conditions for the combustion space must distinguish between the refractory surfaces above glass melt, the port openings as well as the glass bath itself. All three sections require either calculation or prescription of effective temperatures and effective emissivities of the radiating boundaries.

Heat Losses through Refractory Walls

Local surface temperatures of the refractories exposed to the combustion space were calculated with the zone model and with a 1-D model for heat conduction through the refractory walls using effective values for the ratio k/s of conductance to refractory thickness and estimations for outside refractory temperatures.

Calculation of Port Heat Losses

Net radiation through the port openings constitutes a major heat loss of the combustion space. In case of O_2-combustion, the ports were also considered to be open, since the experimental set-up for O_2-conversion of the furnace considered in this study was planned for all ports to be left open. The analysis of port radiation was separately carried out by applying the zone model for a representative section of a port and the upper regenerator.

The port analysis yielded ultimately port view factors, which differed between the cycles for air combustion and also for O_2-combustion. The view factors $F_{f-->rg}$ are defined by Eq. (5)., which relate the net heat flux Q_p through the combustion space port opening with area A_p to the incident radiation q_p, in from the combustion space and to an effective black regenerator temperature $T_{rg,eff}$:

$$Q_p = F_{f->rg} \; A_p \; (q_{p,in} - \sigma T^4_{rg,eff}) \qquad (5)$$

Boundary Conditions at Glass Surface

In prescribing thermal boundary conditions at the melter surface, it was assumed that the glass of the end-section was batch-free. Two different types of thermal boundary conditions were then studied.

In a first set of calculations, a uniform effective temperature $T_{gl} = 2600^{\circ}F$ (1700 K) and an effective emissivity of $\epsilon_{gl} = 0.88$ were used for the whole glass surface. The value used for ϵ_{gl} corresponds to the greys hemispherical emissivity of a transparent glass sheet with infinite optical thickness and a refractive index of 1.7 (Ref. 11).

The second set of calculations was carried out by calculating effective temperatures of the glass surface with help of a simple heat conduction model into the glass. It is assumed that temperatures of the glass are uniform (2410°F = 1600 K) in a horizontal plane located at a certain vertical distance into the bath. A uniform effective ratio of conductance to thickness of the glass layer was then determined so, that the area-weighted effective glass surface temperature was 1700 K (2600F). The surface emissivity used in this approach was again $\epsilon_{gl} = 0.88$.

It is believed, that use of a uniform value for glass surface temperatures simulates closer conditions for a transparent glass, where as the second way to calculate boundary conditions, is more representative for a darker glass. Both approaches are certainly very approximate. However, it has to be pointed out, that predictions of relative performance changes for the air and O_2-system can still be accurate provided similar incident heat flux distributions at the glass bath can be achieved in the O_2-system by appropriate burner selection, placement and operation.

INPUT DESCRIPTION AND CASE DEFINITIONS

Furnace Description

The glass furnace investigated in this study is designed for a pull rate of 350 TPD. The furnace is cross-fired and is currently operated with natural gas using regeneratively heated air as oxidizer. A horizontal cross-section of the furnace is shown in Fig. 3. The furnace is 27.2 ft (8.28 m) wide and 49.6 ft (15.11 m) long. The distance between glass surface and crown is 8.7 ft (2.64 m). Each of the five ports of each furnace side is equipped with two pipe burners with 2.3" nozzle diameters. The burners point from each port side at an angle of 47 degrees relative to the port axis and produce five long flames which extend over the whole furnace width. The time between a switch of the burners of one side to the opposite side is 30 min.

Oxy-fuel Burner

The Linde "A" Burner, patented by Union Carbide Industrial Gases, Inc., was chosen for the oxy-fuel firing cases. The burner offers high momentum low flame temperature characteristics suitable for glass furnaces (Ref. 12). The arrangement of the burners are shown in Fig. 4.

Model Geometry for End-Section

For reasons described in an earlier section, it was decided to conduct the 3-D modeling study of the combustion space for only one section of the furnace, namely the end-section. The space covered by the model, which is indicated in Fig. 3 extends from the center-plane between the fourth and the fifth ports to the bridge-wall. Thus, the model assumes that heat transfer in

the combustion space is symmetrical with respect to the vertical center-plane. In the graphical display of the results following later, this symmetry feature will be utilized by extending the plots of the furnace variables up to the center-plane of the fourth port.

The 3-D zone arrangement used in the heat transfer model of the end-section is displayed in Fig. 4. The zone arrangement utilized basically consists of a 9*6*7 rectangular volume zones with some of the near roof zones distorted or omitted in order to simulate the curvature of the furnace roof.

Thermal Boundary Conditions for End-Section

The thermal boundary conditions considered for the end-section are summarized in Table 1.

A uniform value of 0.5 was assumed for the emissivity of all refractory surfaces. The effective ratios of conductance to wall thickness $(k/s)_{eff}$ as well as the outside surface temperatures for various furnace wall sections were deducted from an heat loss analysis carried out for air operation by a furnace manufacturer. In particular, the ratios $(k/s)_{eff}$ were determined so that the current zone model will predict the same overall heat losses, if the flame side surface temperatures coincide with those used in the heat loss analysis mentioned above.

Table 1 also lists the view factors and effective regenerator temperatures used in Eq. (5) to calculate the port losses for air and O_2 combustion, respectively. The mean values for $T_{rg,eff}$ used in the air case are also supported by measurements of gas and refractory temperatures in the upper regenerator carried out over the whole firing cycle.

The boundary conditions at the glass surface were prescribed as discussed in the general description of the approach. In particular, two sets of calculations were carried out. The first set of calculations was carried out assuming a uniform effective glass surface temperature of 2600°F (1700 K). In the second set of calculations, a constant temperature of 2420°F (1600 K) was assumed to occur someway into the glass bath. A uniform effective ratio of conductance to thickness of k/s = 0.612 kW / m^2 K was used in order to calculate heat transfer through the upper glass bath layer. This value was determined so, that the area weighted glass surface temperatures averaged 2600°F (1700 K) for the baseline O_2 firing configuration. In both set of calculations, an effective glass surface emissivity of 0.88 was utilized.

Major Operating Conditions and Case Definitions

Major operating conditions of the end-section considered for air and O_2-Firing are listed in Table 2. The gross fuel heat input of 12.16 MMBtU/hr (3563 kW) utilized for air firing is related to the gas burners of one port. The fuel heat input cited for O_2 firing relates to half of the fuel input for O_2 burner A5 plus the heat input for O_2 burner A6 (see Fig. 4). The air preheat of 2330°F (1550 K) utilized for conventional air firing corresponds to average measured values for the burner load considered. Similarly, the O_2 concentrations of 2.2 Vol. %, dry corresponds to average O_2 concentrations measured during the flue gas cycle in the upper regenerator.

All cases studied in this paper are defined in Table 3. The 3-D modeling effort comprises five major cases. However, four of these cases are also presented for a variation, in which the glass surface temperatures are calculated from a simple model rather than prescribed to be constant. The cases with constant glass surface temperatures are numbered 1.0 through 5.0, and the cases with variable surface temperatures 1.1 through 5.1.

Case 1 is the case conducted for conventional air combustion and serves, in the context of this study, as bench mark for performance comparisons with predictions of Cases 2 through 5 for the O_2-firing system. The firing arrangement for Case 1 is shown in Fig. 4.

Case 2 through 5 were performed for a latitudinal arrangement of two oxygen burners as shown in Fig. 4. The burners are numbered A5 and A6. A5 fires along the centerline between the two last ports of the glass furnace (Ports 4 and 5). A6 fires in opposite direction with burner axis located in the plane which divides the breast wall section between last port and the bridge wall in half.

Case 2 with equal burner load A5/A6 was performed to optimize the O_2 configuration. All other oxygen cases were performed for burner load ratio A5/A6 of 3.71. Case 3 is defined as baseline with burner directed horizontally and mounted 2 ft (0.610 m) above the glass bath. Case 4 with horizontal burners 1.3 ft (0.396 m) above glass surface was conducted to study the impact of burner elevation. In Case 5 finally, the O_2 burners mounted at 2 ft were angled downwards towards the center-line of the furnace.

RESULTS AND DISCUSSION

Air Case and Model Verification

Results obtained for conventional air firing (Case 1) of the end-section are displayed in Figs. 5 through 8. Fig. 5 shows the relative mass flux distribution utilized in horizontal and vertical cross-sections of the furnace. The flow is

characterized by a weak outer recirculation field surrounding the forward flow emerging from the firing port. The recirculation eddy extends over the whole furnace depth. Its strength was prescribed to be 1.0 times the inlet mass flow. However, previous experience with the zone model has shown that, in weak recirculating flows like in the current air case, the actual recirculation strength has only a weak effect on thermal performance provided bulk flow features are approximately simulated.

Fig. 6 shows the distributions of gas temperatures (F) predicted for air firing in a horizontal and in a vertical furnace cross-section through the flame as well as in a vertical cross-section located halfway between Port 5 and the bridge wall. The predicted flame extends over the whole furnace depth up to the flue gas port. This agrees with observations made in the actual furnace. It was observed that sooty flame tips extended intermittently into the opposite port. The mean gas exit temperature predicted is 2851°F (1840 K). This is in good agreement with optical pyrometer measurements, which yielded averaged gas temperatures near the flue gas port of ca. 2857°F (1843 K) as seen from the regenerator observation ports.

Fig. 7 shows the distribution of refractory temperatures (F) predicted for all walls of the furnace end-section for air firing. In this graph, as well as in all following graphs for air combustion, the display of the variables (i.e. the refractory temperatures in this case) is symmetrized with respect to the furnace axis. This approximately accounts for the complete firing cycle. Maximum refractory temperatures of 2684°F predicted for the furnace roof fall into the range of measured mean crown temperatures, which varied from 2650°F for the section of Port 1 to 2850°F for the end-section (Port 5). The maximum roof refractory temperature of the non-symmetric prediction was 2694°F (1752 K). In comparing the model predictions with the behavior of the actual furnace, one has to consider that the actual fuel distribution between the port burners was not uniform. Furthermore, the actual furnace volume is larger than that the virtual volume of twice the end-section considered in the current model set-up.

Some gradients of predicted refractory temperatures are due to the fact that the refractory material and outer insulation differed from section to section. This effect is especially obvious for the uninsulated tuckstones located just over the glass surface. Relatively low surface temperatures are predicted for these stones.

Fig. 8a shows the symmetrized net heat flux distribution predicted at the glass surface for air combustion and assuming uniform effective temperatures of the glass surface of 2600°F (1700 K). The shape and the inhomogeneity of these heat flux profiles indicate a considerable influence of direct flame radiation on overall heat transfer to the glass. The heat fluxes

to the glass vary from maximal 98 kW/m^2 below the flame to less than 40 kW/m^2 adjacent to the bridge wall.

O_2-Burner Load Optimization and O_2 Base Case

In the first step carried out to optimize the O_2-firing configuration, the thermal load of the A5 and A6 O_2 burners of the end-section (see Fig. 4) was considered to be equal (Case 2). The resulting net heat flux distribution to the glass surface is shown in Fig. 8b. Like in the air case, the O_2-flames generate a radiation image on the glass surface. Maximum heat fluxes of 114 kW/m^2 predicted for flame A5 was slightly higher than those predicted for air combustion.

However, by comparing Fig. 8b with Fig. 8a, it is obvious, that the glass surface section near the bridgewall receives too much heat in the O_2 case. If two glass surface sections are defined so that Section 1 is the glass area between the center-lines of Ports 4 and 5 and Section 2 is the remaining area up to the bridge wall, then the heat flux ratio between Sections 1 and 2 is 1.54 for air Case 1 compared to only 1.03 for O_2 Case 2. Furthermore in the O_2 case, maximum refractory temperatures of the bridge wall exceeded the ones predicted for air Case 1 by 67°F (37 K).

In order to lower the bridge wall temperatures and in order to achieve a heat flux ratio between Sections 1 and 2 which is more similar to that predicted for air combustion, the load ratio A5/A6 was increased from 1 in Case 2 to 3.71 in Case 3. This resulted in an increase of the heat flux ratio between Sections 1 and Sections 2 from 1.03 to 1.31 . It also led to a local heat flux distribution at the glass surface, which is more similar to that predicted for air Case 1 (Compare Fig. 9b with Fig. 9a), and lowered maximum bridgewall temperatures from 2725°F (1769 K) to 2696°F (1753 K). The O_2 case with load ratio A5/A6 = 3.71 was consequently defined as baseline O_2 Case 3.

Further results for the baseline O_2 Case 3 are depicted in Figs. 10 through 12. Fig. 10 shows the relative mass flux distribution of the baseline O_2 case determined for the horizontal and two vertical cross-sections through the axes of Burners A5 and A6. Note, that the mass flux density vectors shown in this figure were plotted in a scale ten times smaller than in corresponding Fig. 5 for the air case.

Derivation of the flow patterns displayed in Fig. 10 is based on enclosed jet theory and flow superposition as described earlier. In particular, a recirculation strength of 15 times the inlet jet mass was utilized for both O_2 jets. Fig. 10 shows that the jets do not significantly influence each other, however, due to its much higher absolute mass flow, jet A5 determines the flow direction in recirculation regions. These features were confirmed in 3-D fluid dynamics calculations carried out independently for the burner configuration of Case 3.

Gas temperature distributions (F) predicted for the O_2 baseline Case 3 in horizontal and vertical burner planes are depicted in Fig. 11. Due to the high recirculation rates, maximum flame temperatures of 3432°F (2162 K) are only slightly higher than those predicted for air combustion (3364°F = 2124 K). These gas temperature maxima are found in Flame A5 which is hotter than Flame A6 due to its much higher load.

Fig. 12 shows the refractory temperatures predicted for O_2 Case 3 at all walls of the furnace end-section. Maximum refractory temperatures of the roof are with 2732°F (1773 K) ca. 48 R (27 K) higher than those predicted for air combustion (Fig. 6). There is a clear correlation between the location of the maximum refractory temperatures and the adjacent gas flow. Maximum refractory temperatures are encountered there, where the gas flow vectors, especially in the flame tail, are directed towards the walls. In O_2 Case 3, these areas are the breastwall region opposite to the A5 burner and the roof section adjacent to this breastwall area. This behavior is less noticeable for Burner A6 due to the shorter high temperature flame zone.

A similar correlation can be found between near wall flow direction and maximum heat fluxes, although the heat flux peaks are influenced as well by bulk radiation effects. Fig. 8b shows, that, compared to O_2 Case 2 with burner load ratio A5/A6 = 1 (Fig.7b), maximum heat fluxes to the glass shifted nearer to the opposite breastwall of Burner A5 and are found in the region, where the flame envelope touches the glass surface. The weaker relative heat flux maximum associated with Flame A6 is located more towards the center of the furnace due to the shortness of the high temperature zone of this flame.

Impact of O_2-Burner Elevation and Burner Angling

It is clear from the previous statements, that burner positioning and angling must have some influence on maximum refractory temperatures, on net heat flux distribution to the glass and on overall heat transfer efficiency. In order to investigate these influences, O_2 Cases 4 and 5 were conducted.

In Case 4, both the A5 and the A6 burners remained horizontally directed, but were lowered from 2 ft above glass surface to only 1.3 ft over glass surface. The impact of burner elevation on net heat flux distribution is shown in Fig. 12, which compares the results obtained for Case 4 with the heat fluxes predicted for the baseline O_2 Case 3. By lowering the burners from 2 ft to 1.3 ft, peak heat fluxes at the glass increased from 115 kW/m^2 to 122 kW/m^2. This increase is accompanied by a decrease of peak roof refractory temperatures by 15 R (8 K).

A still more dramatic effect on heat flux distribution to the glass is obtained when the O_2-burners are angled towards the glass surface in direction of the furnace center-line (Case 5). The relative mass flux distribution utilized in this case is shown in Fig. 13. Fig. 14 shows the gas temperature distributions predicted for the angled O_2 flames. Compared to the horizontal O_2 flames of the baseline case (Fig. 10), maximum flame temperatures decreased by ca. 150 (F). This is an indication for an improved heat transfer to glass surface. The net heat flux distribution at the glass surface produced by the angled flames is depicted in Fig. 15b. Compared to the baseline Case 3 (Fig. 15a), maximum heat flux densities increased from 115 kW/m^2 to 131 kW/m^2 and, as can be expected, the location of the heat flux maximum of each flame shifted more towards its corresponding burner wall. The increase of peak heat fluxes is accompanied by an overall increase of heat transfer efficiencies (see section on overall performance).

The angling of the O_2-burners also causes a considerable redistribution of refractory temperatures as shown in Fig. 16. Compared to the distribution for the baseline O_2 Case 3 (Fig. 11), maximum roof refractory temperatures are lowered by 20 R (11 K) and the location of roof peak fluxes has shifted towards Burner A5. However, the stronger flow along the glass after impingement of jet A5 on the glass surface causes an increase of maximum breast wall temperatures by 40 R (22 K) compared to the baseline O_2 case.

Effect of Variable Glass Surface Temperatures

The preceding results, which were obtained using a uniform effective surface temperature of the glass, showed relative large in homegenities in the distribution of net heat fluxes at the glass surface. Largest and smallest net heat fluxes of 95 kW/m^2 and 35 kW/m^2, respectively, were for instance predicted for air combustion (Case 1), and of 110 kW/m^2 and 40 kW/m^2 for the baseline O_2 case (Case 3). For the O_2-cases in particular, the local heat flux distributions at the glass surfaces were to a certain extent mirror images of the gas temperature distribution within the O_2-flames.

Considerably flatter net heat flux distributions are predicted, when the glass near the surface responds to the imprint of the net heat flux distributions through change of its temperature. This effect is modelled by the simple model for variable glass surface temperatures . Results obtained from this model are shown in Fig. 18a for air combustion and in Fig. 18b for the baseline O_2 burner configuration. In case of air combustion and variable glass temperatures (Case 1.1), largest and lowest heat fluxes are only 83 kW/m^2 and 47 kW/m^2, respectively. Similarly, for the baseline O_2 Case with variable glass surface temperatures (Case 3.1), highest and lowest heat fluxes amount to 80 kW/m^2 and 50 kW/m^2, respectively.

Resulting distributions of calculated effective surface temperatures for air Case 1.1 and baseline O_2 Case 3.1 are compared in Figs. 19a and 19b., respectively. Peak glass temperatures $T_{s,gl,max}$ for air combustion reach 2663°F (1735 K) and the differences between this peak and the lowest temperatures predicted is $dT_{s,gl}$ = 105 R (59 K). For O_2 combustion, these numbers are $T_{s,gl,max}$ = 2656°F (1731 K) and $dT_{s,gl}$ = 90 R (50 K), respectively.

As it can be expected, in all cases investigated with variable glass surface temperatures, maximum refractory temperatures increased by about 10 K (20F) compared to corresponding cases assuming a uniform effective glass surface temperature. The higher peak refractory temperatures are offset by lower refractory temperatures in furnace corners, especially in the O_2 cases which exhibit a somewhat more inhomogeneous refractory temperature distribution. This can be seen in Figs. 20 and 21 which display the refractory temperature distribution predicted for the air Case 1.1 and for the O_2 Case 3.1, respectively.

OVERALL PERFORMANCE COMPARISON AND CONCLUSIONS

Overall heat transfer performance data predicted for all cases is listed in Table 4. Note, that the fuel heat input cited in this table, is calculated with the lower calorific value. Table 1 confirms the known fact, that overall heat transfer efficiency of the O_2-firing system is improved compared to conventional air combustion. For the O_2-firing systems studied, this increase is achieved without significant increase in maximum flame temperatures and maximum refractory temperatures. Although the air flames are wider than the O_2 jet flames, the discrepancy in size of the O_2 flames is offset by much higher mixing and recirculation rates induced by the O_2-burners.

It is also obvious from Table 4, that positioning and angling of the O_2-burners can influence overall performance to a certain degree. Lowering the burners (Case 3) slightly increases heat transfer efficiency to the glass surface. A somewhat stronger improvement is achieved when the burners are angled towards the glass surface. In this case, heat transfer efficiency is increased by 0.5 percentage points compared to the baseline O_2 case with horizontal burner orientation.

The study also showed, that there is certainly an impact of the glass surface thermal properties on heat transfer in the combustion space itself. A darker glass will likely tend to smooth out local inhomogenties of net heat fluxes to the glass by increase of glass surface or near surface temperatures, thus reducing the effect of the firing system or of the burner placement on heat flux distribution.

Although some of the absolute predictions made in the present study may be inaccurate due to simplifications of the current approach, there is little doubt that the general trends concluded from this study are realistic. This is due to the dominance of radiation on overall heat transfer in the high temperature glass furnace, and radiative exchange is treated very accurately by the current model.

ACKNOWLEDGEMENT

This work was jointly funded by the U. S. Department of Energy and Union Carbide Industrial Gases, Inc. under Contract No. DE-FC07-88ID12833. The authors would like to express appreciation to Mr. J. Keller of EG&G and Mr. R. N. Chappell of the U. S. Department of Energy for their support and advice.

REFERENCES

[1] J. Brown, et. al., "Oxygen-Fuel Fired Glass Furnace," Amer. Ceramic Society, Glass Division, Pacific Coast Regional Meeting, Nov. 1-3, 1987.

[2] Shamp, D.E. and Davis, D. "Application of 100% Oxygen Firing at Parkersberg, W.V." H.A. Nelson Memorial Glass Seminar, Louisville, KY, April 11, 1990.

[3] Nolet, D. A., and R. A. Murnane. Development of Modeling Techniques for Glass Furnaces. 1st International Conference on Advances in th Fusion of Glass. Alfred University, New York, June 14-17, 1988, pp. 13.1 - 13.21

[4] Ungan, A. and Viskanta, R., "State-of-the-Art Numerical Simulation of Glass Melting Furnaces," Ceramic Eng. Sci. ProC., 9 [3-4], pp. 203-220 (1988).

[5] Carvavalho, M. G., P Oliveira and V. Semiao. A Three-Dimensional Modelling of an Industrial Glass Furnace. J. Inst. Energy, 1988, 448, pp. 143-156.

[6] Richter, W., and M. P. Heap. A Semistochstic Method for the Prediction of Radiative Heat Transfer in Combustion Chambers. Western States Section, The Combustion Institute, 1981 Spring Meeting, Paper 81-17, 1981.

[7] Richter, W., Scale-Up and Advanced Performance Analysis of Boiler Combustion Chambers. 1985 ASME Winter Annual Meeting, Paper 85-WA/HT-80, 1985.

[8] Smith, T. F., and Z. F. Shen. Evaluation of Coefficients for the Weighted Sum of Gray Gases Model. 20th Joint ASME/AICHE National Heat Transfer Conference, Paper 81-ht-55, 1981.

[9] Johnson, T. R., and J. M. Beer. The Zone Method Analysis of Radiant Heat Transfer: A Model for Luminous Radiation. J. Inst. Fuel, Vol 46, 1973, p 388.

[10] Richter, W., and R. Payne. Modeling Study of Burner and Furnace Performance for Oxygen Enriched Combustion Systems. AFRC 1988 Spring Meeting, May 10-11, 1988, Toronto, Canada.

[11] Gardon, R. A review of Radiant Heat Transfer in Glass. J. of the American Ceramic Society. Vol. 44., No. 7, July 1961

[12] Anderson, J.E., "A Low NO_x Low Temperature Oxygen Fuel Burner," 1986 Symposium on Industrial Combustion Technologies, Chicago, IL, Apr. 29-30, 1986.

List of Tables

List of Figures

TABLE 1 : INPUT PARAMETERS FOR BOUNDARY CONDITIONS AT REFRACTORY WALLS, PORTS AND GLASS SURFACE

PARAMETER	DIMENSION		POSITION / COMMENT
REFRACTORY WALLS :			
EMISSIVITY	-	0.5	ALL SECTIONS
EFF. RATIO COND./THICKNESS	W/M**2 K	2.496	BRIDGE W. (NOT J=1 ZONES)
		0.701	MELTER CROWN (EXEPT SKEWS OVER PORT I= 3,4 ZONES)
		2.329	SKEWS OVER PORTS (I=3,4)
		0.615	BREAST WALLS (EXCEPT J=1)
		6.997	TUCKSTONES (J=1 ZONES, BUT NOT BELOW PORTS)
		13.333	TUCKSTONES BELOW PORTS (J=1)
EFF. OUTER SKIN TEMP.	F	341	BRIDGE W. (NOT J=1 ZONES)
		212	MELTER CROWN (EXEPT SKEWS OVER PORT, I= 3,4 ZONES)
		294	SKEWS OVER PORTS (I=3,4)
		255	BREAST WALLS (EXCEPT J=1)
		511	TUCKSTONES (J=1 ZONES, BUT NOT BELOW PORTS)
		742	TUCKSTONES BELOW PORTS (J=1)
PORTS :			
VIEW FACTORS :			
AIR FLUE CYC.		0.30	
AIR AIR CYC.		0.57	
O2 - FIRING		0.33	
REG. TEMP. T RG			
AIR FLUE CYC.	F	2510	
AIR AIR CYC.	F	2420	
O2 - FIRING	F	2366	CASES 2.0, 3.1, 3.2, 3.3
O2 - FIRING	F	2465	ALL OTHER O2 CASES
GLASS SURFACE :			
EMISSIVITY	-	0.88	ALL CASES
EFF. SURFACE TEMPERATURE	F	2600	CASES 1.0 THROUGH 5.0,
EFF. RATIO COND./THICKN. OF UPPER GLASS LAYER	W/M**2 K	612	CASES 1.1 THROUGH 5.1 (SURFACE TEMPERATURES CALCULATED ASSUMING 2420 F IN GLASS BATH)

TABLE 2 : MAJOR OPERATING CONDITIONS FOR SECTION CONSIDERED FOR AIR AND O2-FIRING

PARAMETER	DIMENSION	AIR COMBUSTION	O2 - COMBUSTION
FUEL TYPE	-	NATURAL GAS	NATURAL GAS
UP. CAL. VALUE	BTU/SCF BTU/LB KJ/KG	1010 21674 50414	1013 21674 50414
LOW. CAL. VALUE	BTU/LB KJ/KG	19535 45439	19535 45439
GROSS FIRING RATE	MMBTU/HR MMBTU/HR KW KW	60/5 = 12.5 3519 	CASE 2 : 12.5 ALL OTH. : 12.0 CASE 2 : 3519 ALL OTH. : 3388
NET FIRING RATE	MMBTU/HR MMBTU/HR KW KW	10.8 3172 	CASE 2 : 10.8 ALL OTH. : 10.4 CASE 2 : 3172 ALL OTH. : 3053
OXIDISER TEMP.	F K	2330 1550	77 298
FUEL TEMP.	F K	77 298	77 298
FLUE GAS O2	VOL.%,DRY	2.2	2.2

TABLE 3 : CASE DEFINITIONS

Case Nr.	Type of Oxidiser	Burner Load Ratio A5/A6	Burner El. above Glass	Burner Direction	Eff. Glass Temperature
			FT		F
1	Air	-	1.85	Horizontal	2600
2	02	1.00	2.00	Horizontal	2600
3	02	3.71	2.00	Horizontal	2600
4	02	3.71	1.30	Horizontal	2600
5	02	3.71	2.00	Angled	2600
1.1	Air	-	1.85	Horizontal	Variable
3.1	02	3.71	2.00	Horizontal	Variable
4.1	02	3.71	1.30	Horizontal	Variable
5.1	02	3.71	2.00	Angled	Variable

TABLE 4 : OVERALL PERFORMANCE COMPARISONS FOR END SECTION

Case Nr.	Description	T gas, max	Tcrown, max	T s, glass, max	T s, glass mean	q glass, max	Q fuel+ Q sens, in *)	Q sens, out	Q refr	Q port	Q glass	(Qglass /Qfuel) *100	Q Sec.1 / Q Sec.2 *)
		F	F	F	F	kW/m**2	kW	kW	kW	kW	kW	%	-
1	Air, Base	3331	2684	2600	2600	120.5	3172+ 1790	2701	138	117	2006	63.24	1.54
2	02, 2ft A5/A6=1.0	3650 **)	2697	2600	2600	130.0 **)	3172	822	139	111 ***)	2100	66.20	1.03
3	02, Base, 2ft A5/A6=3.7	3432	2709	2600	2600	115.1	3053	817	138	84	2014	65.97	1.31
4	02, 1.3 ft A5/A6=3.7	3459	2693	2600	2600	121.8	3053	812	138	89	2015	66.00	1.26
5	Case 3, but Burn. Angled	3277	2697	2600	2600	131.2	3053	808	138	80	2027	66.39	1.32
1.1	Air Case 1, Ts,glass Var.	3337	2718	2678	2607	82.6	3172+ 1790	2714	138	127	1983	62.52	1.24
3.1	02 Case 3, Ts,glass Var.	3437	2719	2656	2606	76.1	3053	820	139	121 ***)	1973	64.63	1.15
8	02 Case 4, Ts,glass Var.	3464	2712	2674	2605	86.2	3053	815	138	114 ***)	1986	65.05	1.14
9	02 Case 5, Ts,glass Var.	3277	2705	2708	2606	97.7	3053	808	138	115 ***)	1992	65.25	1.15

*) Heat fluxes calculated until symmetry plane through axis of Burner A5, but heat flux section ratio calculated as defined in text.

**) This calculation was conducted for different flow field with lower recirculation rates leading to somewhat higher gas temperatures and maximum heat fluxes.

***) Calculation conducted for effective regenerator temperatures of 2366 F instead of 2465 F in the other 02 cases

Figure 1 : SEMISTOCHASTIC RADIATION MODEL

TERMINATION:

$$\Delta \dot{Q}_l < \Delta \dot{Q}_{ref}$$

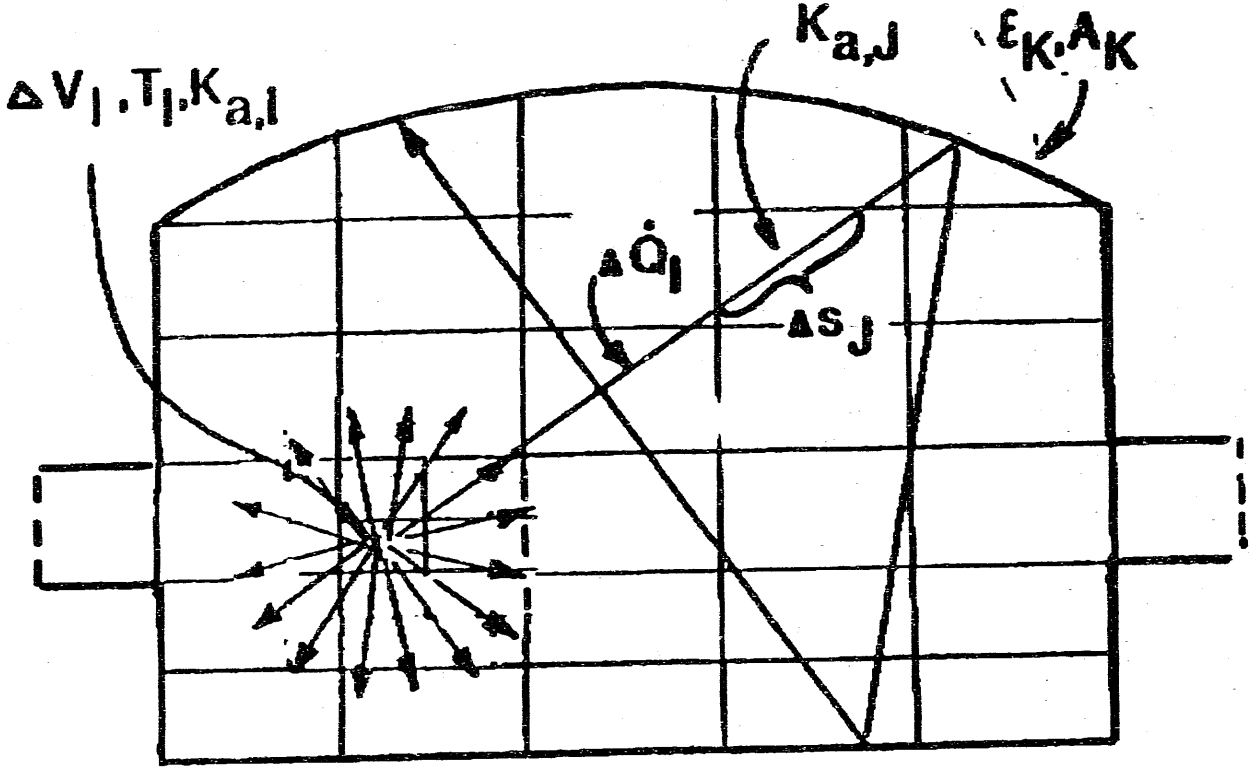

EMISSION:

$$\Delta \dot{Q}_{l,o} = K_{a,l} \frac{\sigma}{\pi} T_l^4 \Delta V_l \Delta \Omega$$

REFLECTION:

$$\Delta \dot{Q}_l = (1-\varepsilon_K)\, \Delta \dot{Q}_l$$

ABSORPTION:

$$\Delta \dot{Q}_{a,K} = \varepsilon_K \Delta \dot{Q}_l$$

$$\Delta \dot{Q}_{a,J} = \Delta \dot{Q}_l \,(1-e^{-K_{a,J}\Delta s_j})$$

ATTENUATION:

$$\Delta \dot{Q}_l \equiv \Delta \dot{Q}_l e^{-K_{a,J}\Delta s_j}$$

RADIATION BALANCE:

$$\dot{Q}_{e,l} - \dot{Q}_{a,l} = \sum_{o}^{nl} K_{a,J} \frac{\sigma}{\pi} T_l^4 V_l \Delta\Omega - \sum_{o}^{ne} \Delta \dot{Q}_{a,l}$$

CALCULATION IN WEIGHTED GRAY O

SPECTRAL RANGES POSSIBLE

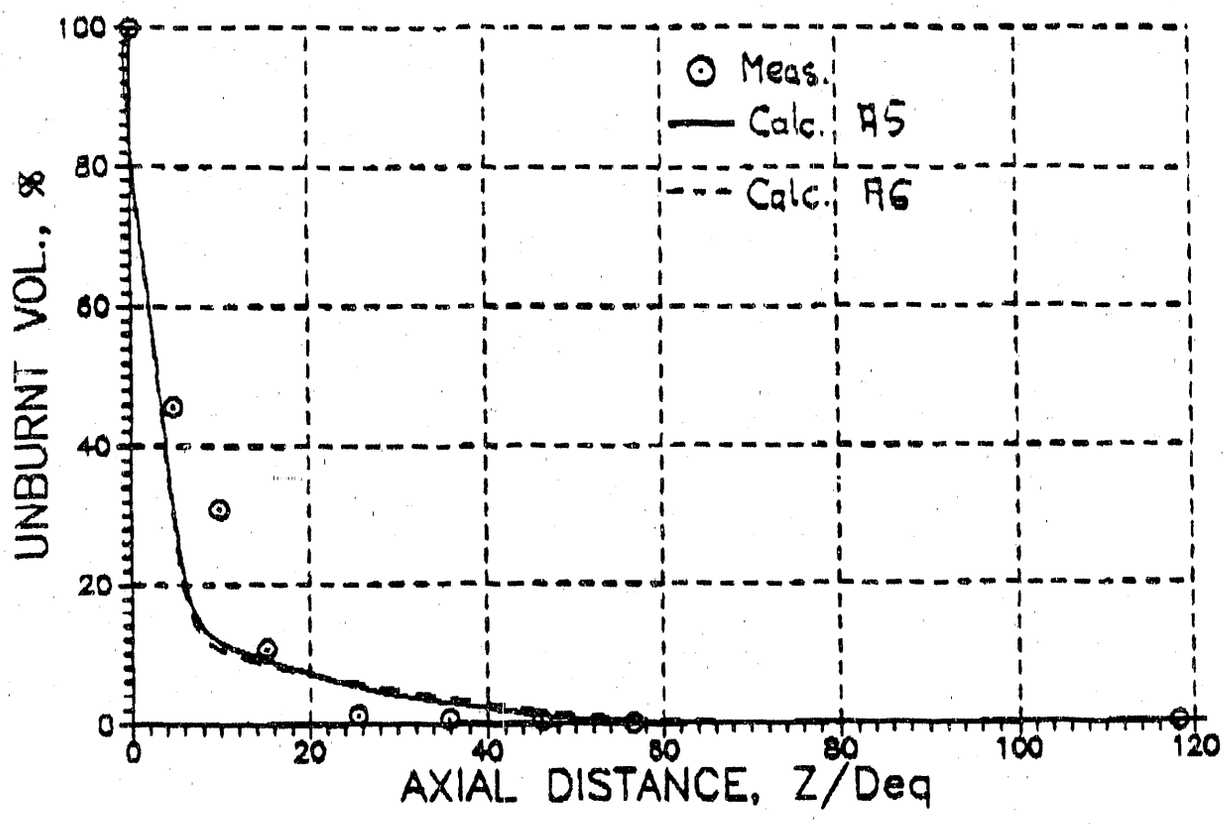
UNBURNT VOL., %
AXIAL DISTANCE, Z/Deq
Meas.
Calc. A5
Calc. A6
0
20
40
60
80
100
120

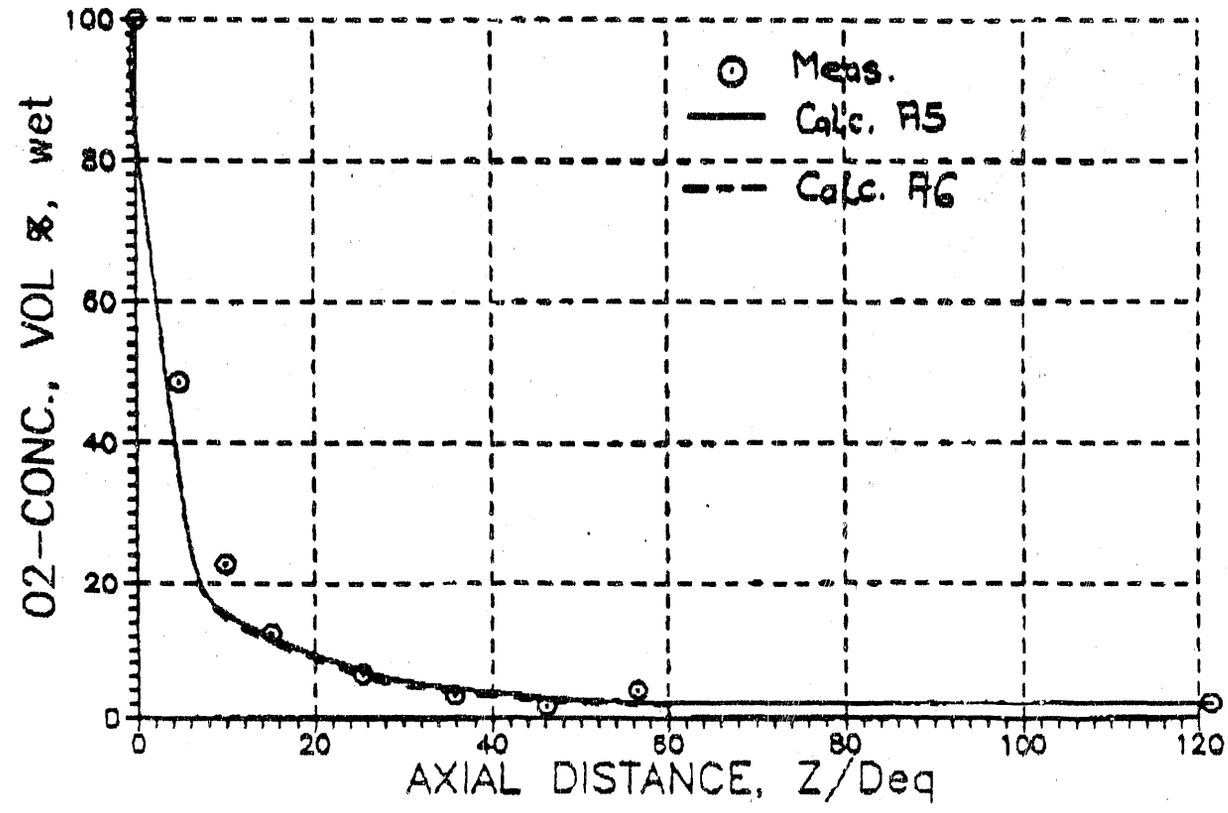
O2-CONC., VOL %, wet
AXIAL DISTANCE, Z/Deq
Meas.
Calc. A5
Calc. A6
0
20
40
60
80
100
120

Figure 2 :

Figure 3 :

PLANE VIEW OF FURNACE & BURNER PLACEMENT

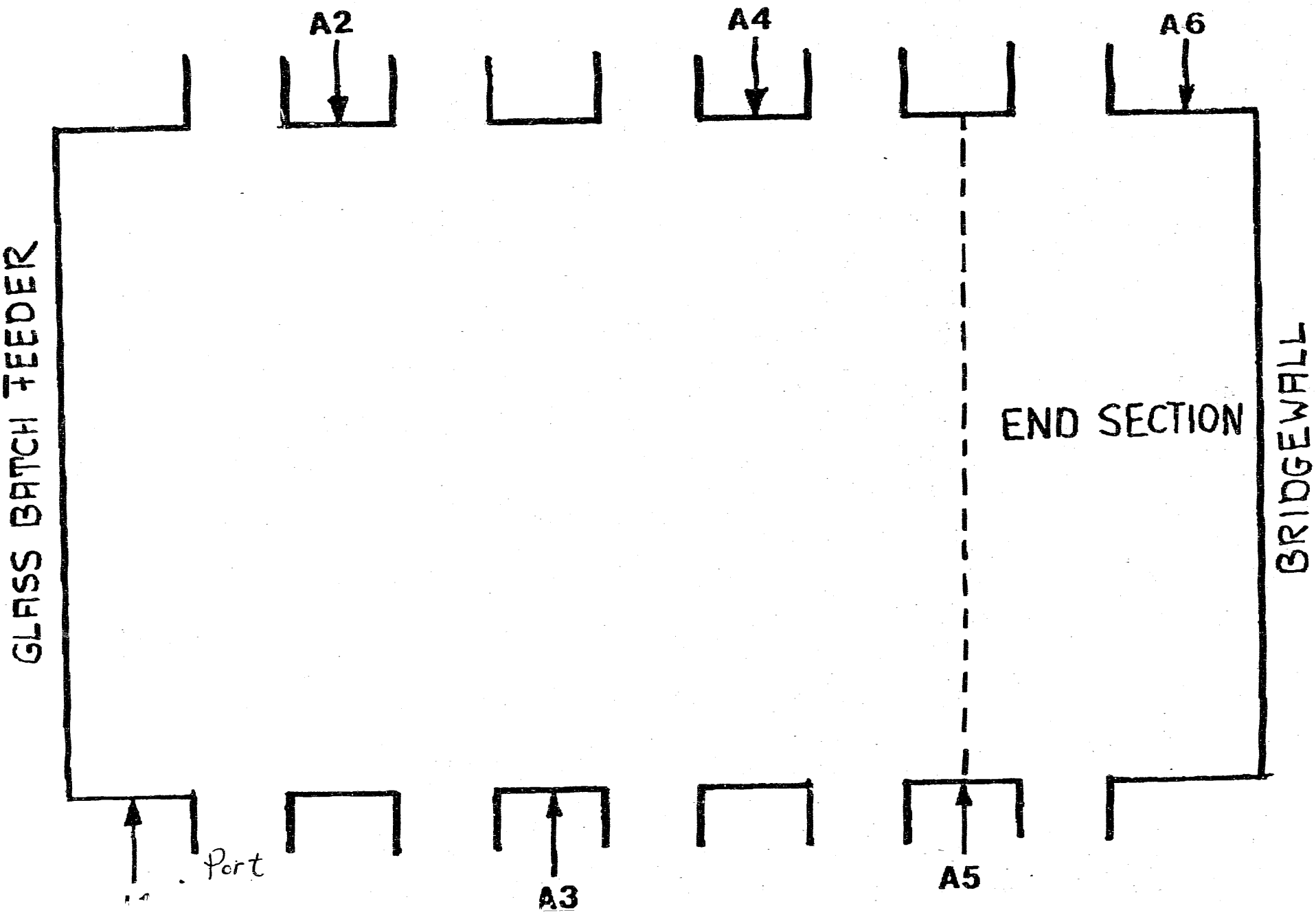

Figure 4:

ZONE ARRANGEMENT FOR FURNACE END SECTION

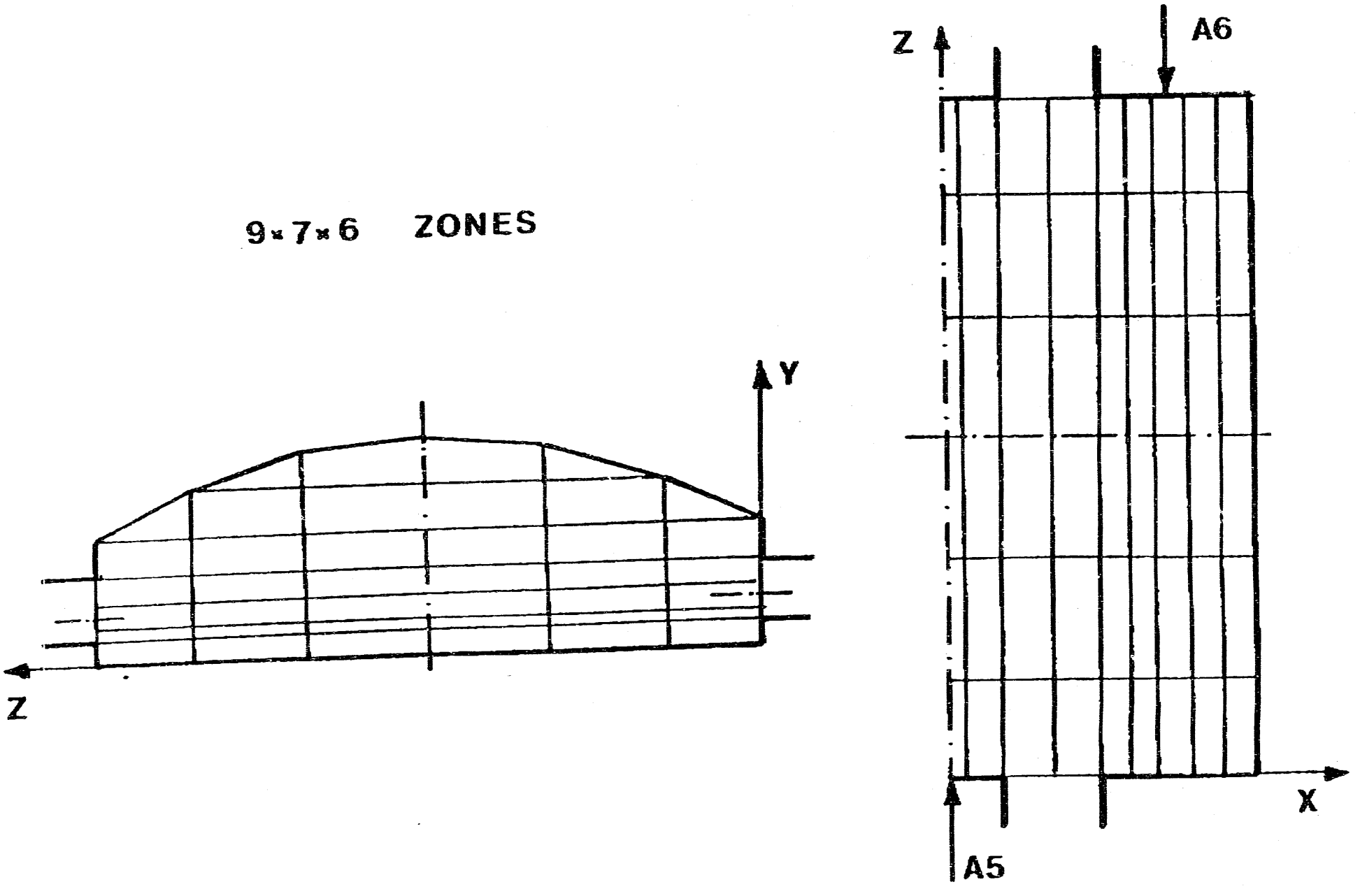

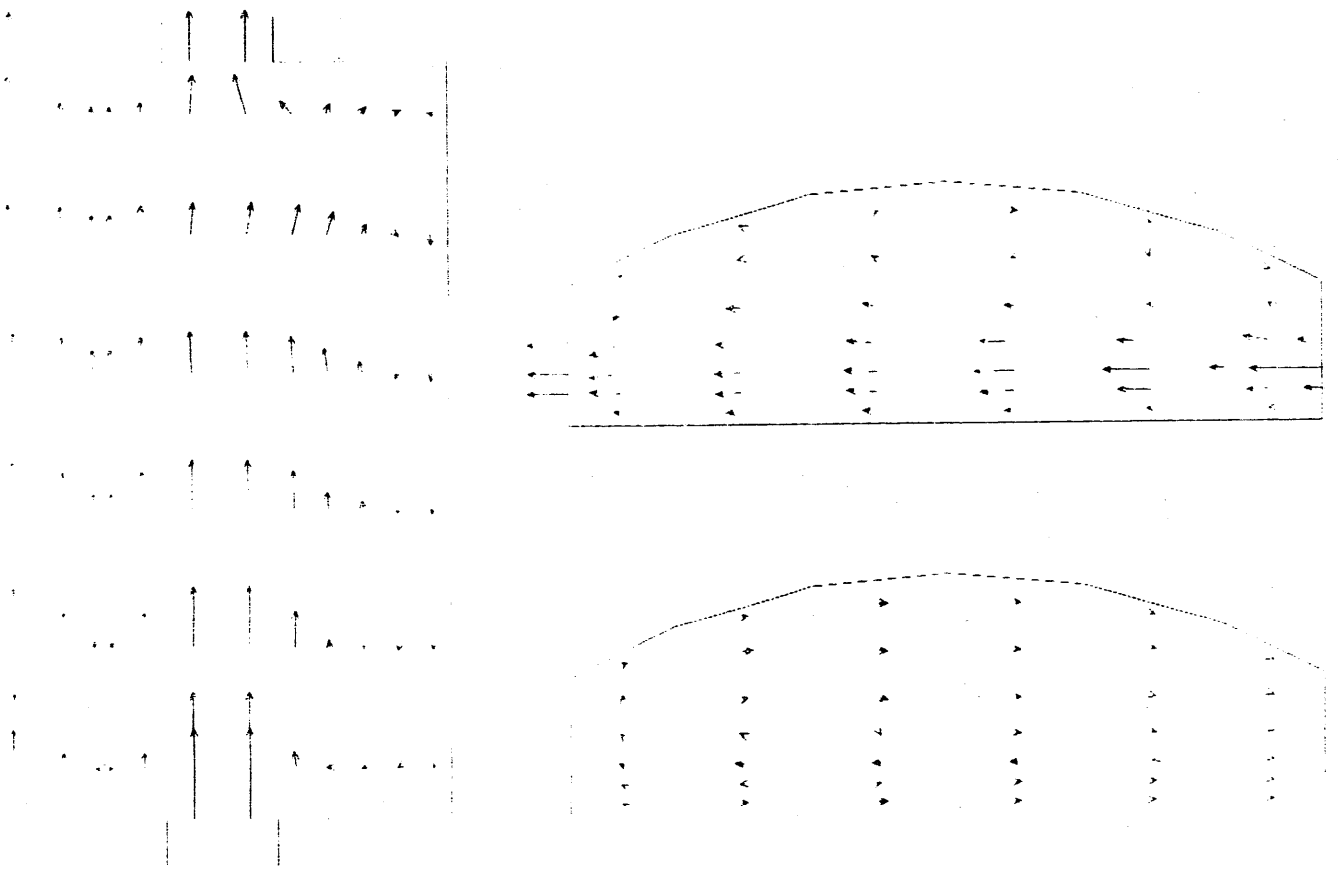

Fig 5

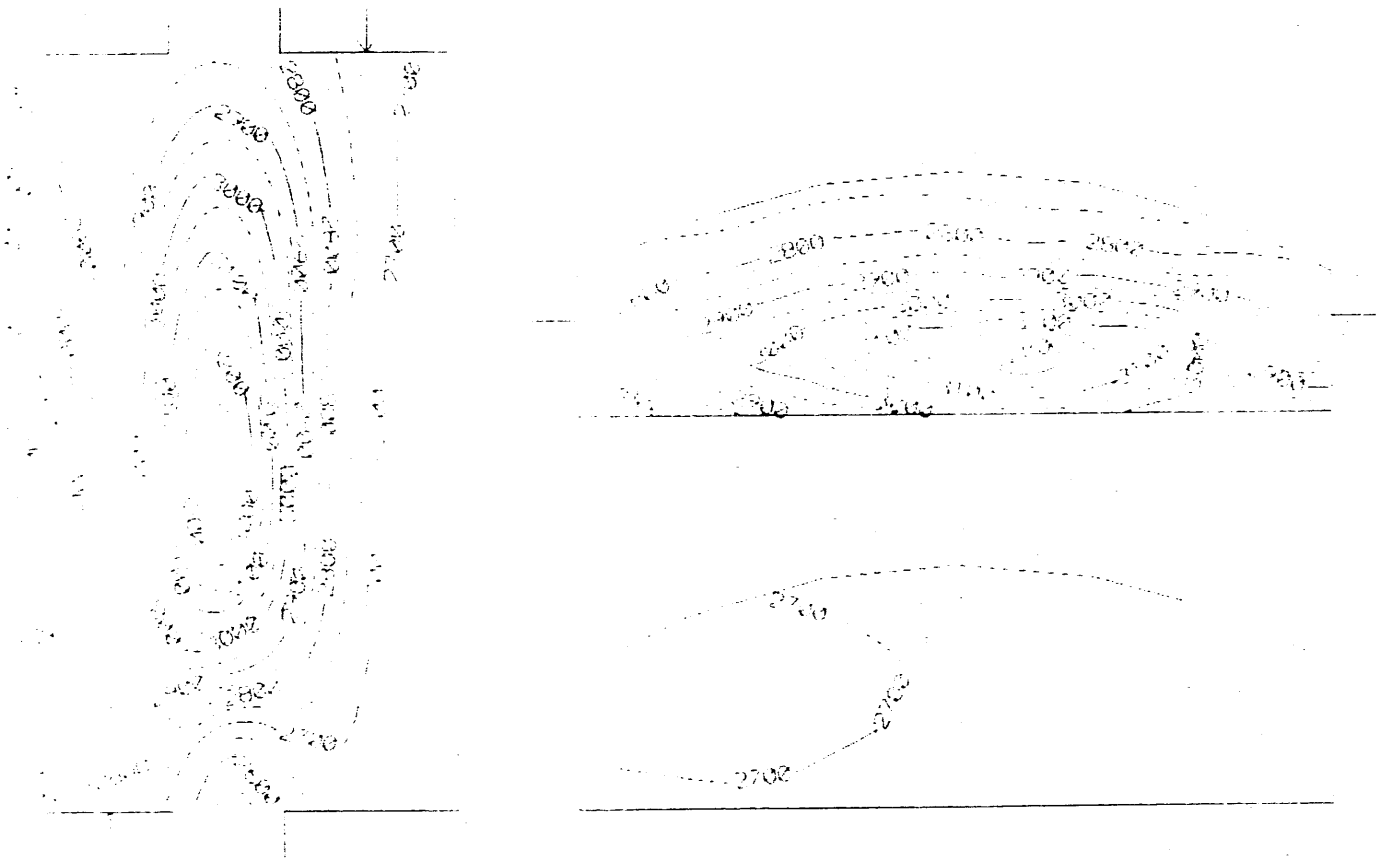

Fig 6.

Fig 7.

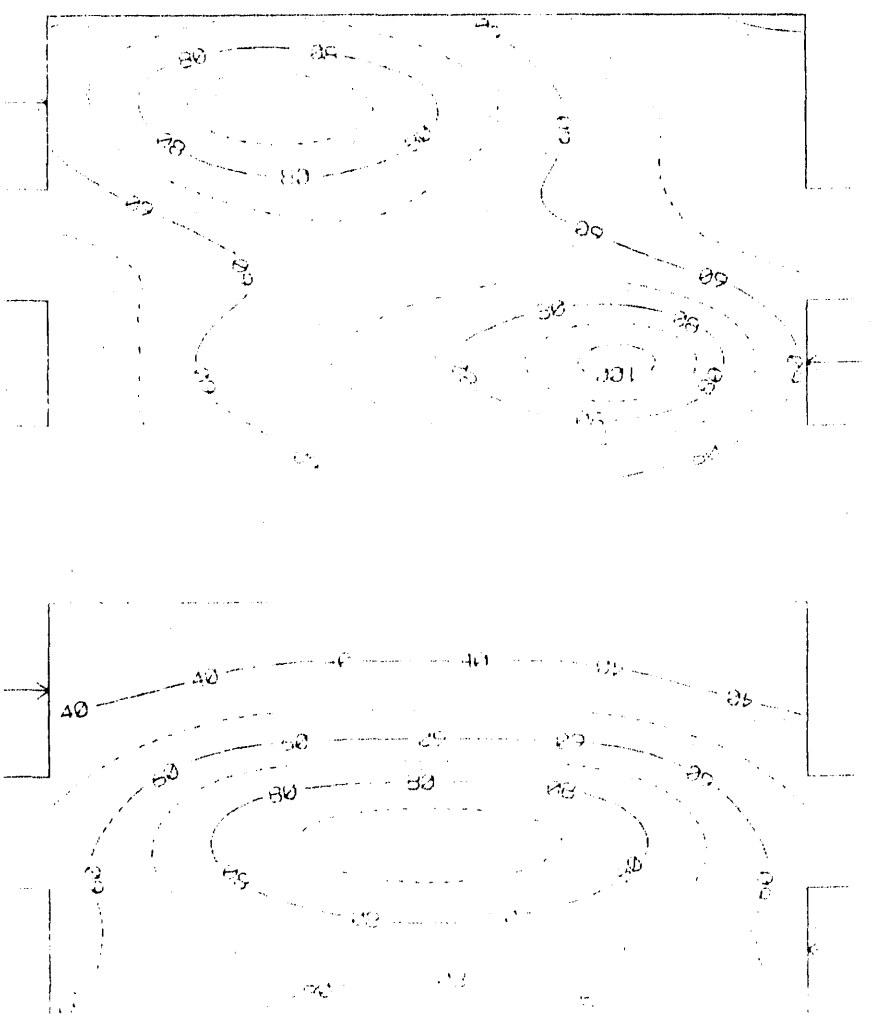

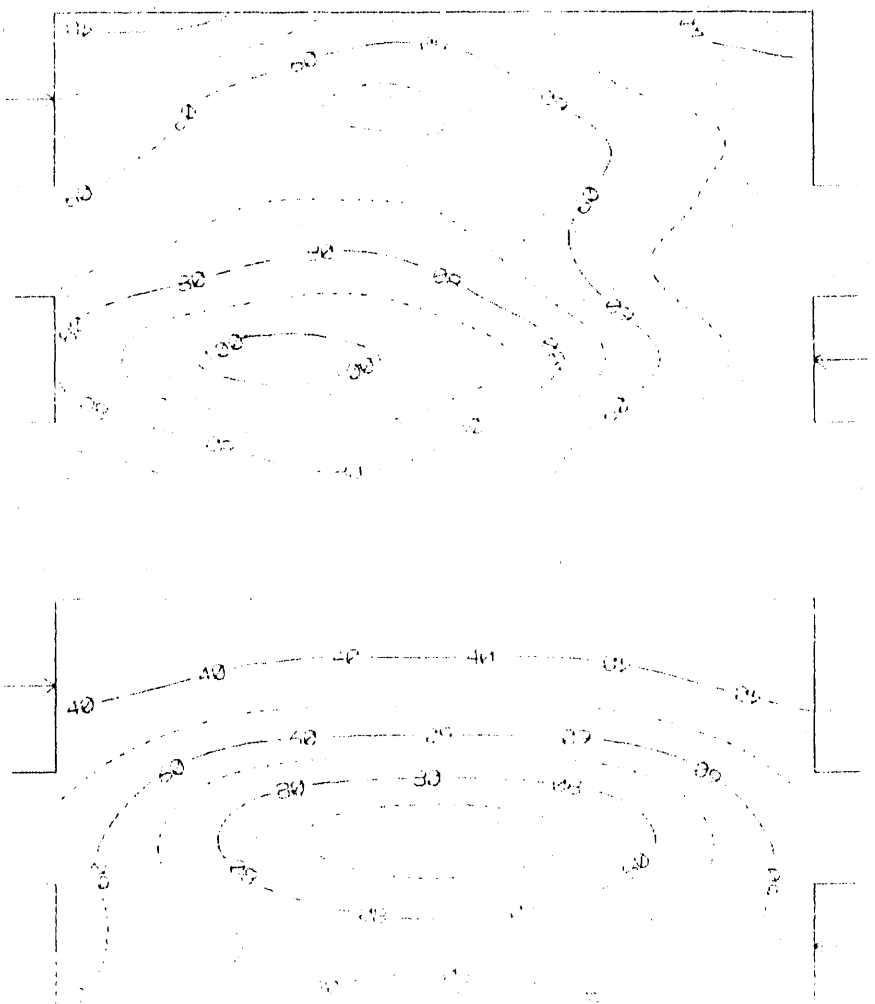

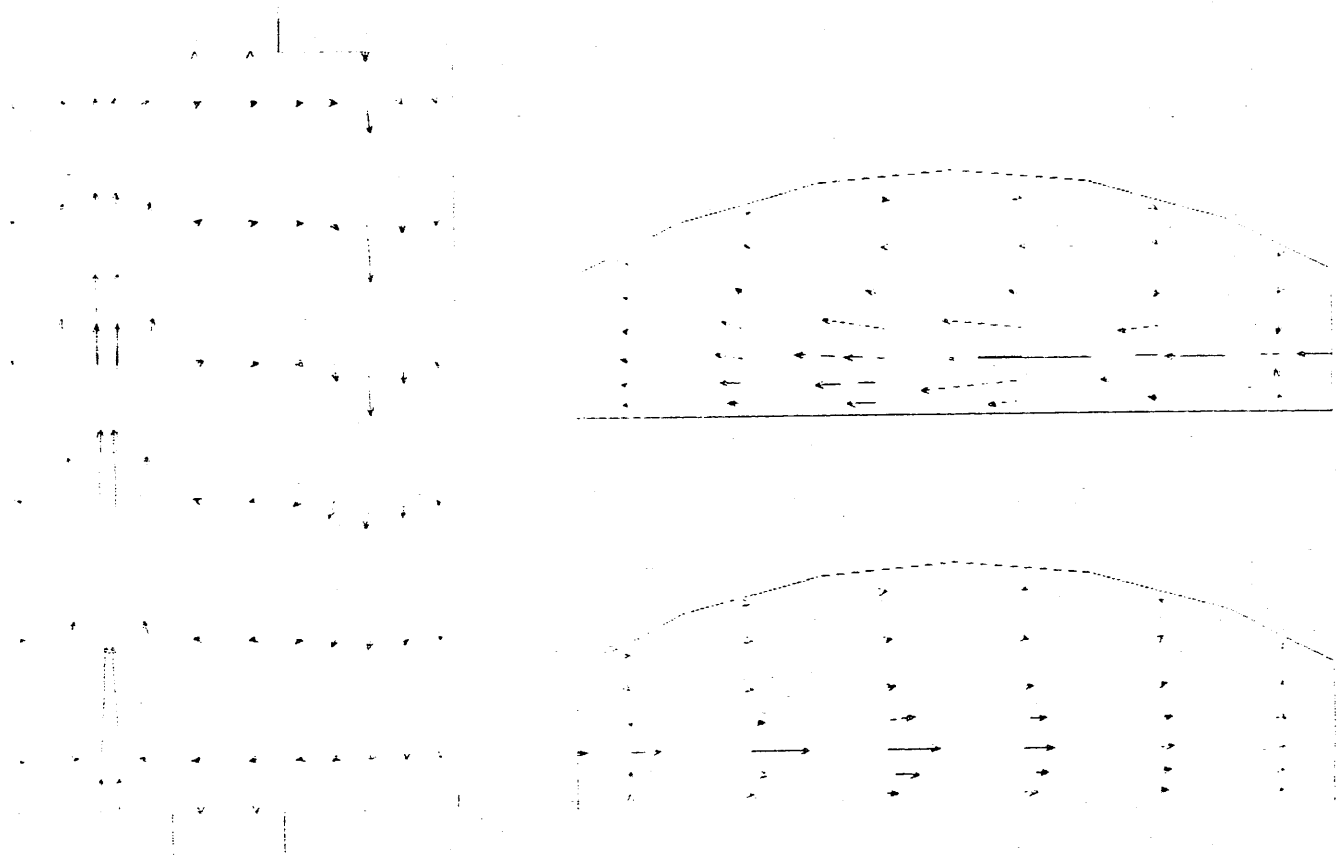

Fig 10

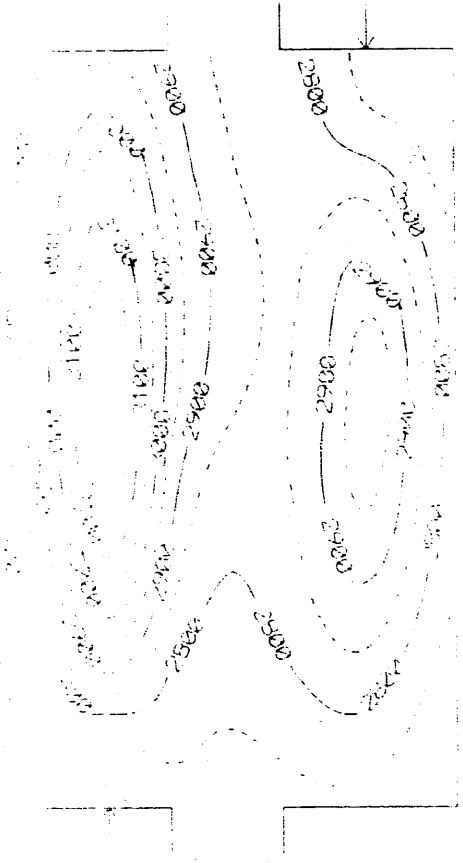

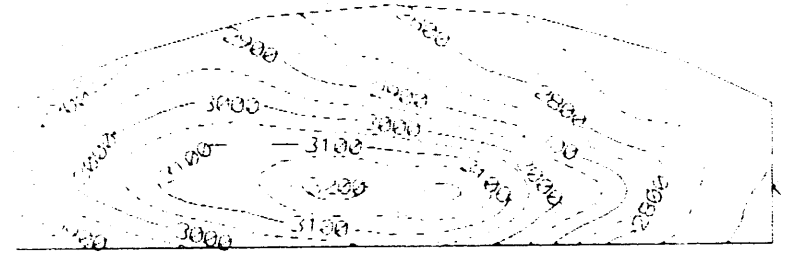

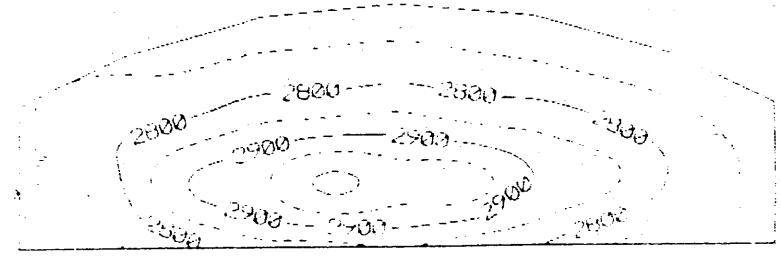

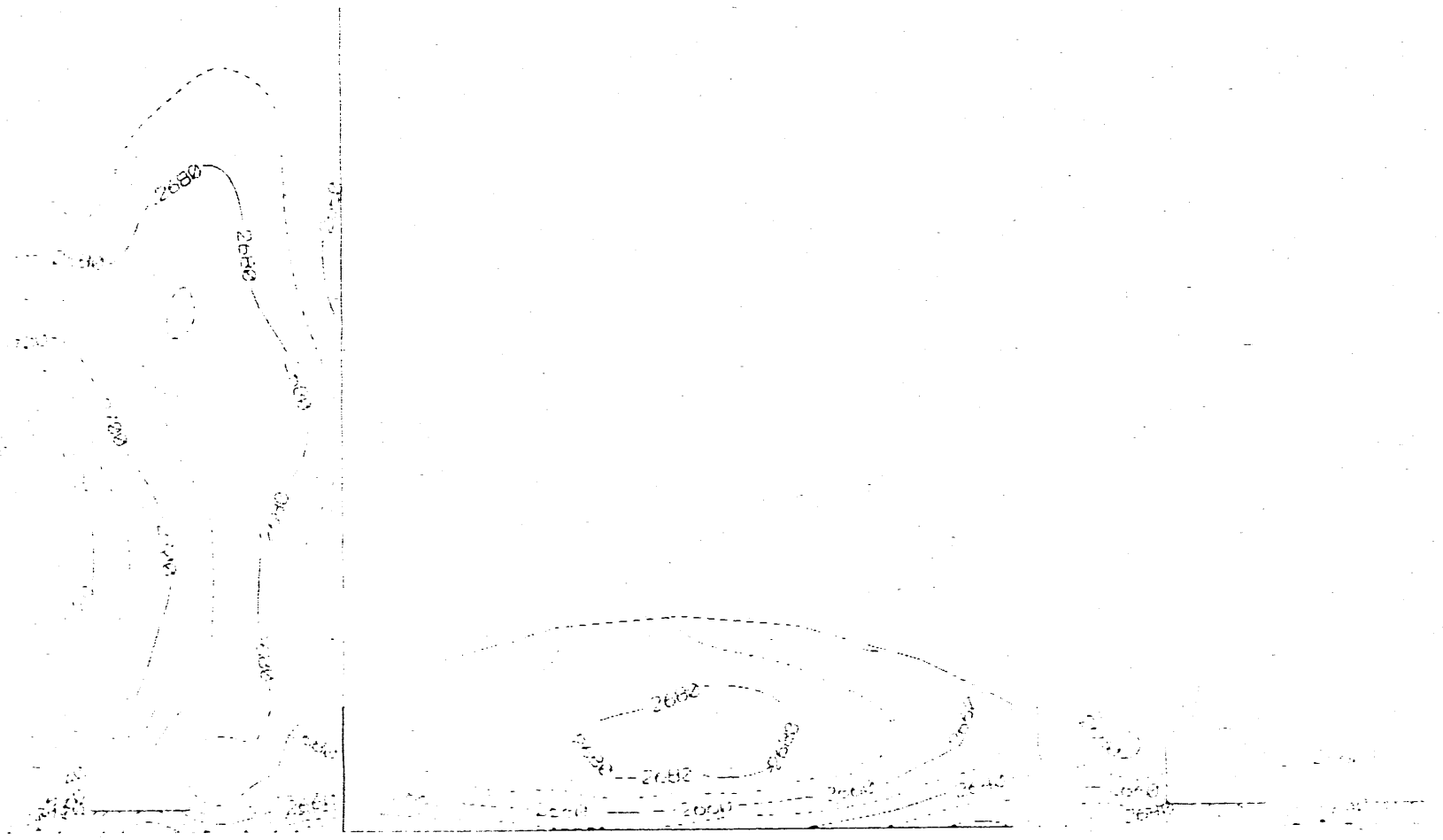

Fig. 1

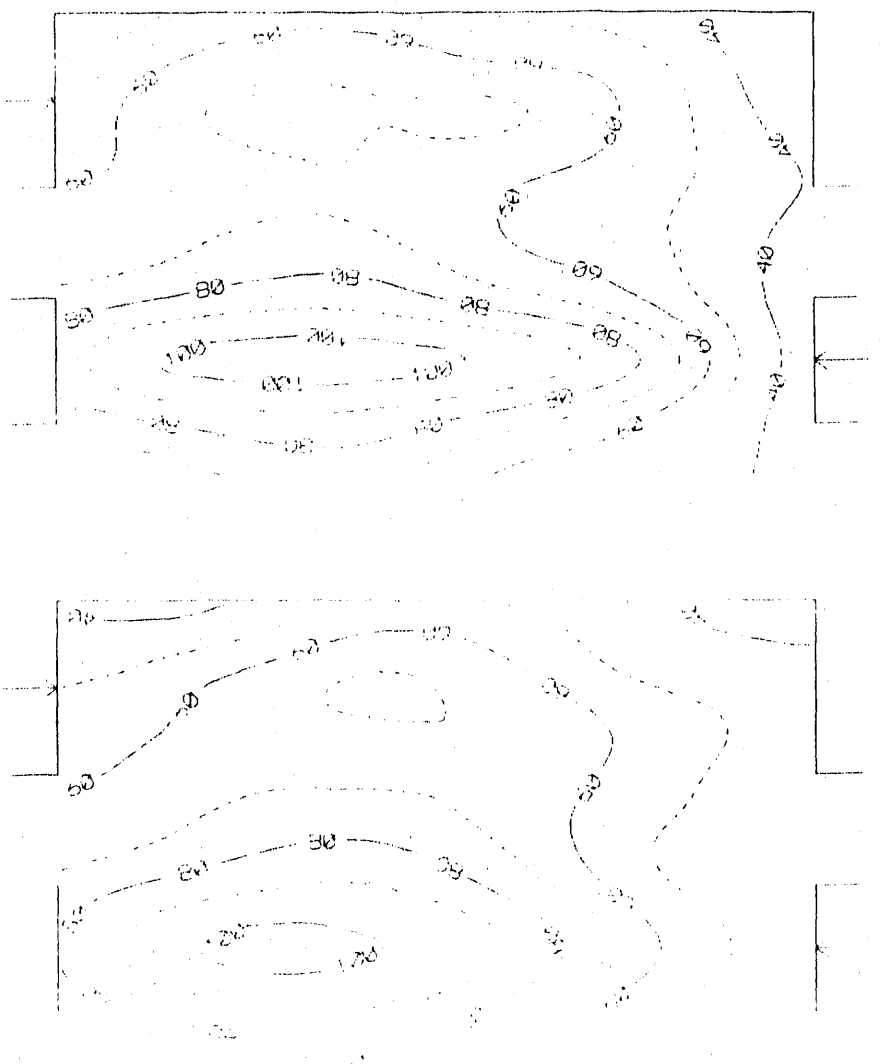

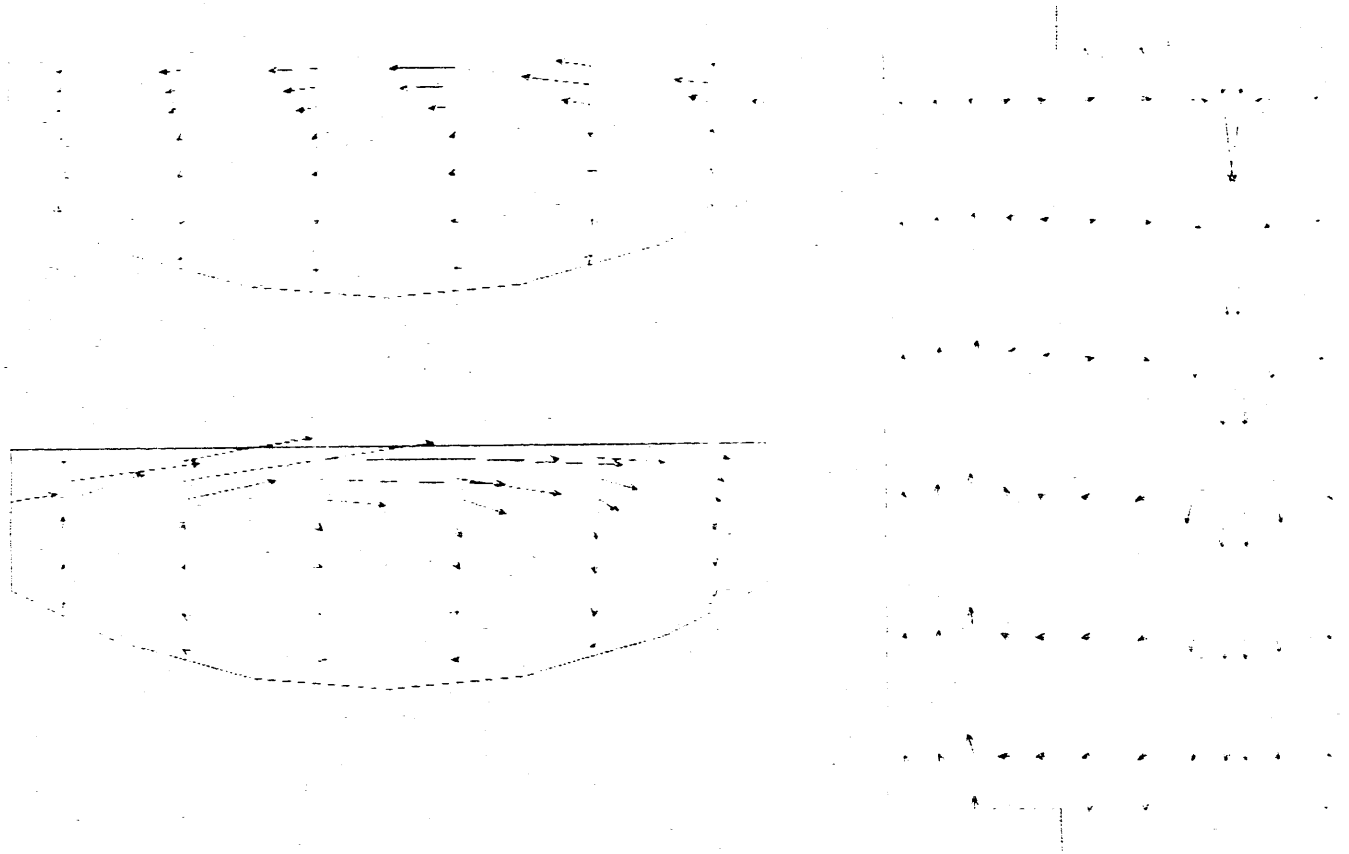

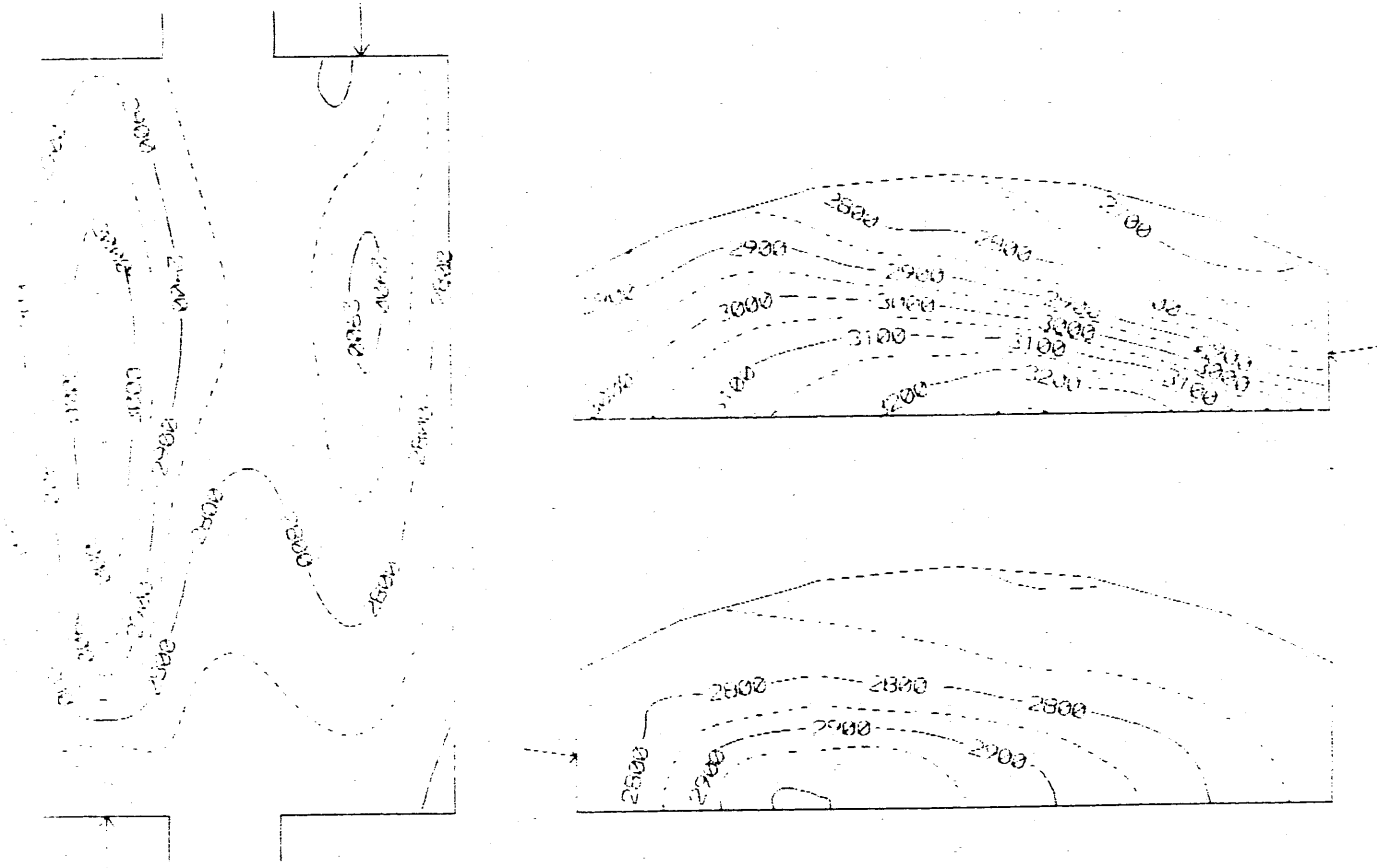

Fig 15

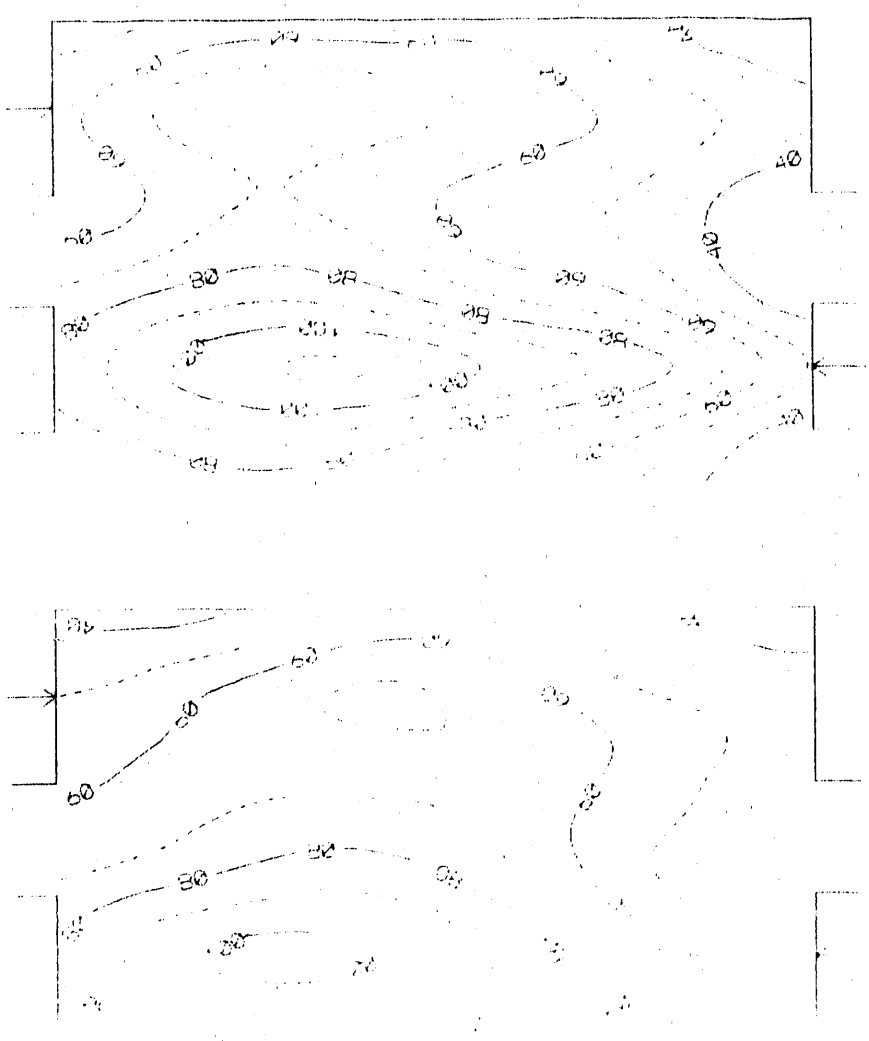

Fig 16

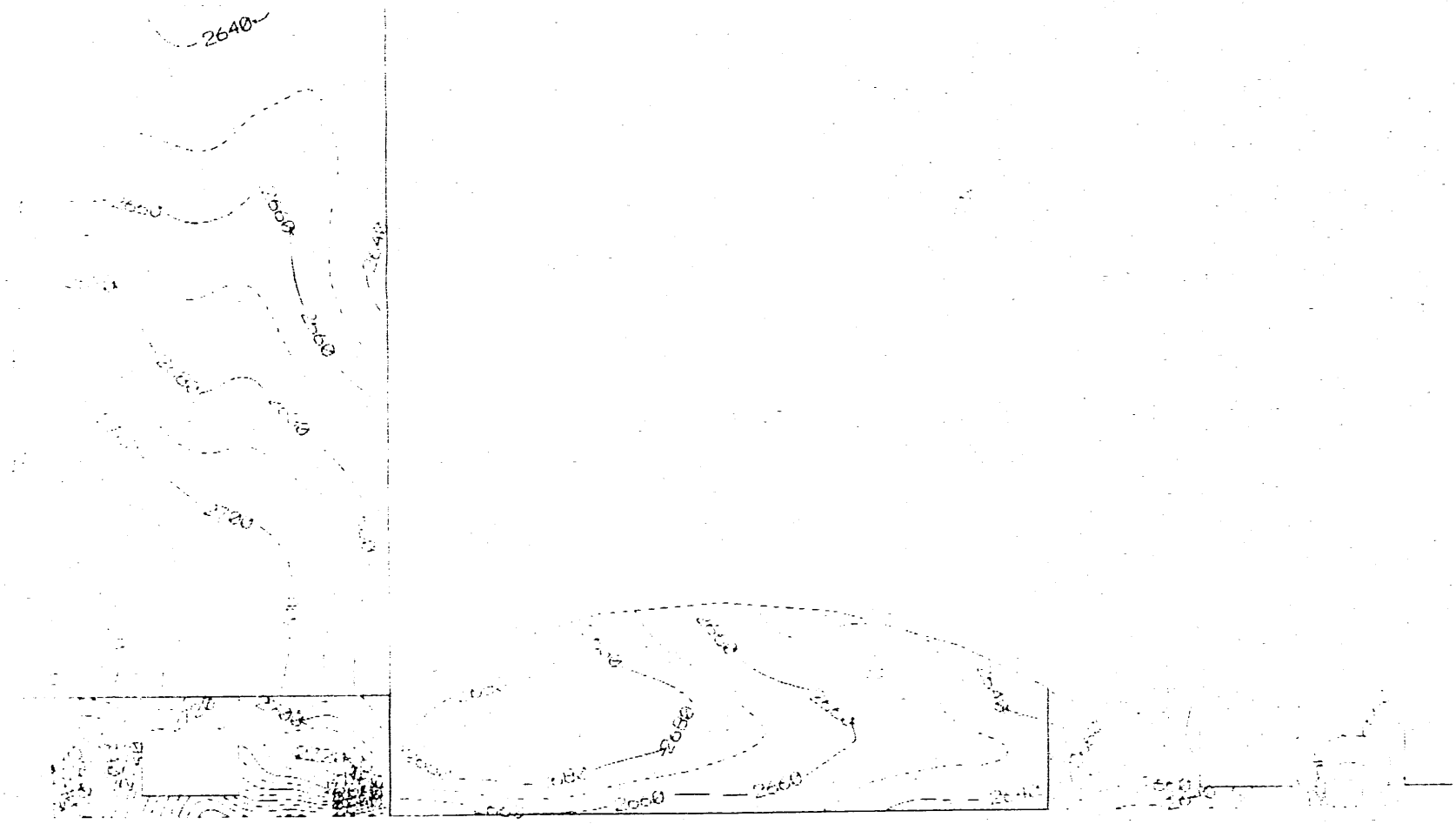
2640
2600
2560
2520
2480
2440
2400
2360
2320
2280
2240
2200
2160
2120
2080
2040
2000

Fig 17

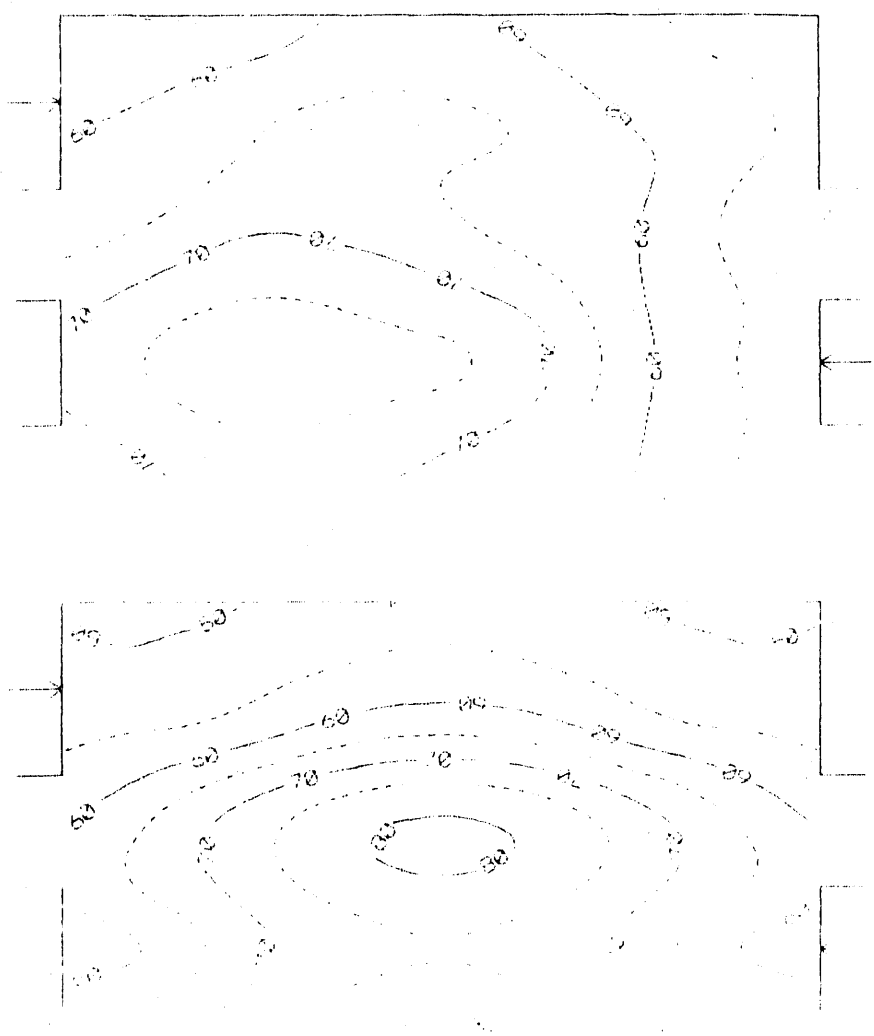

Fig 15

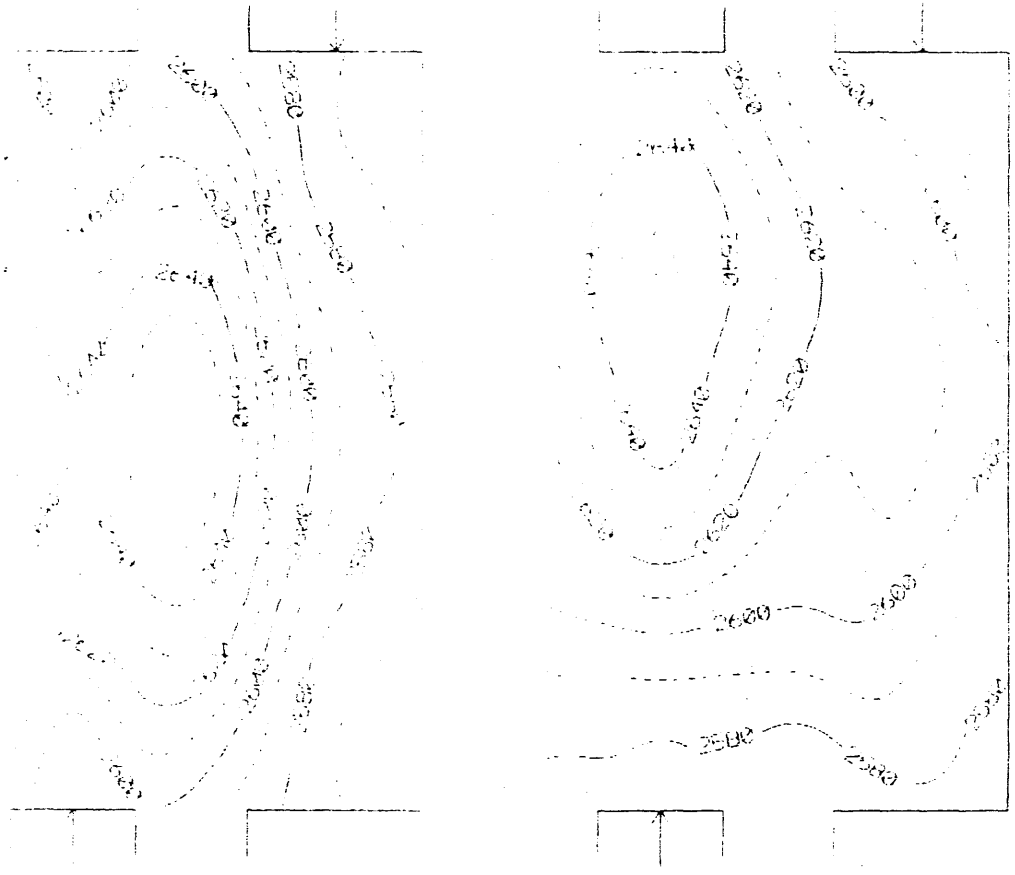

FIG 19

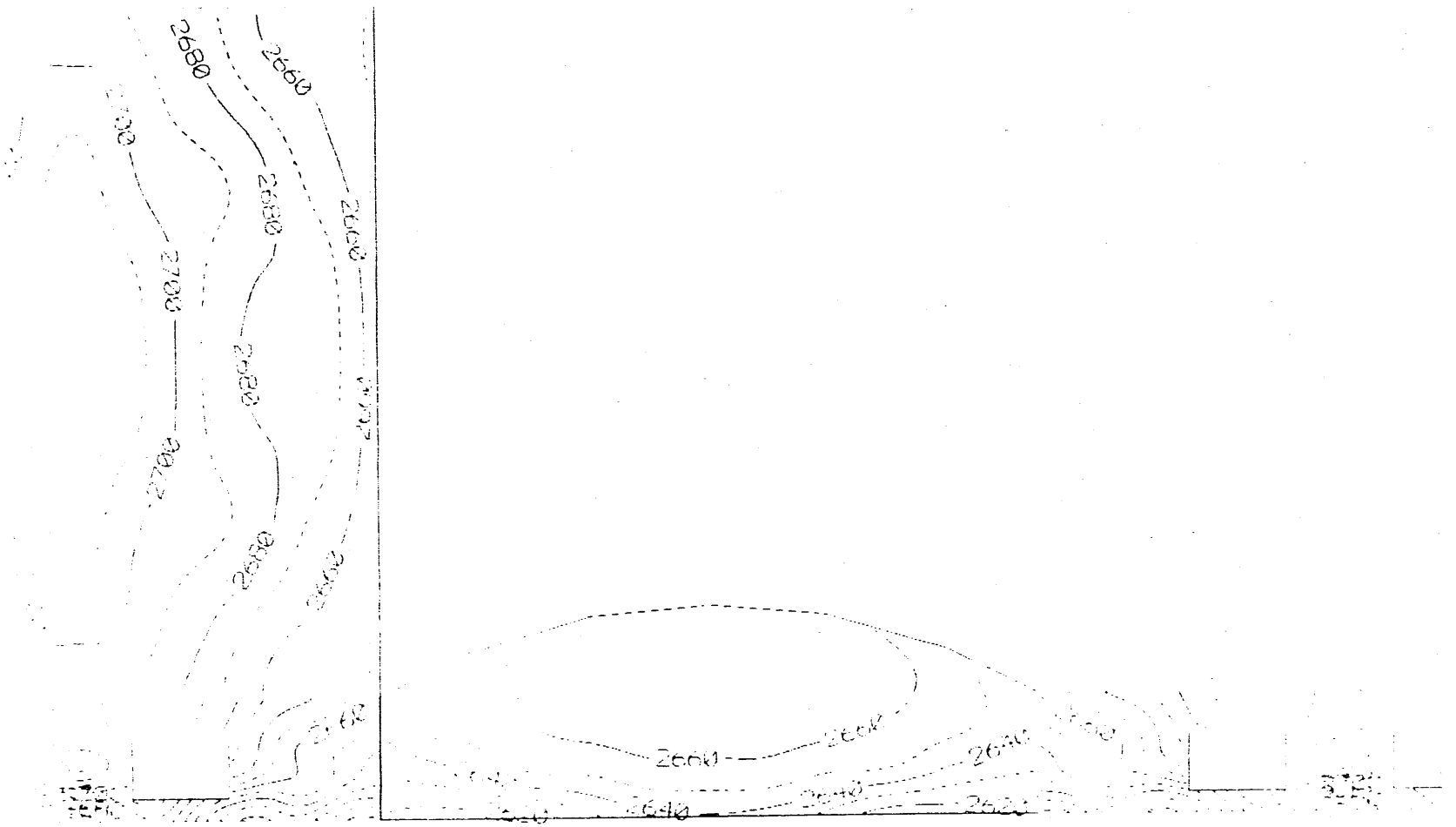

Fig 20

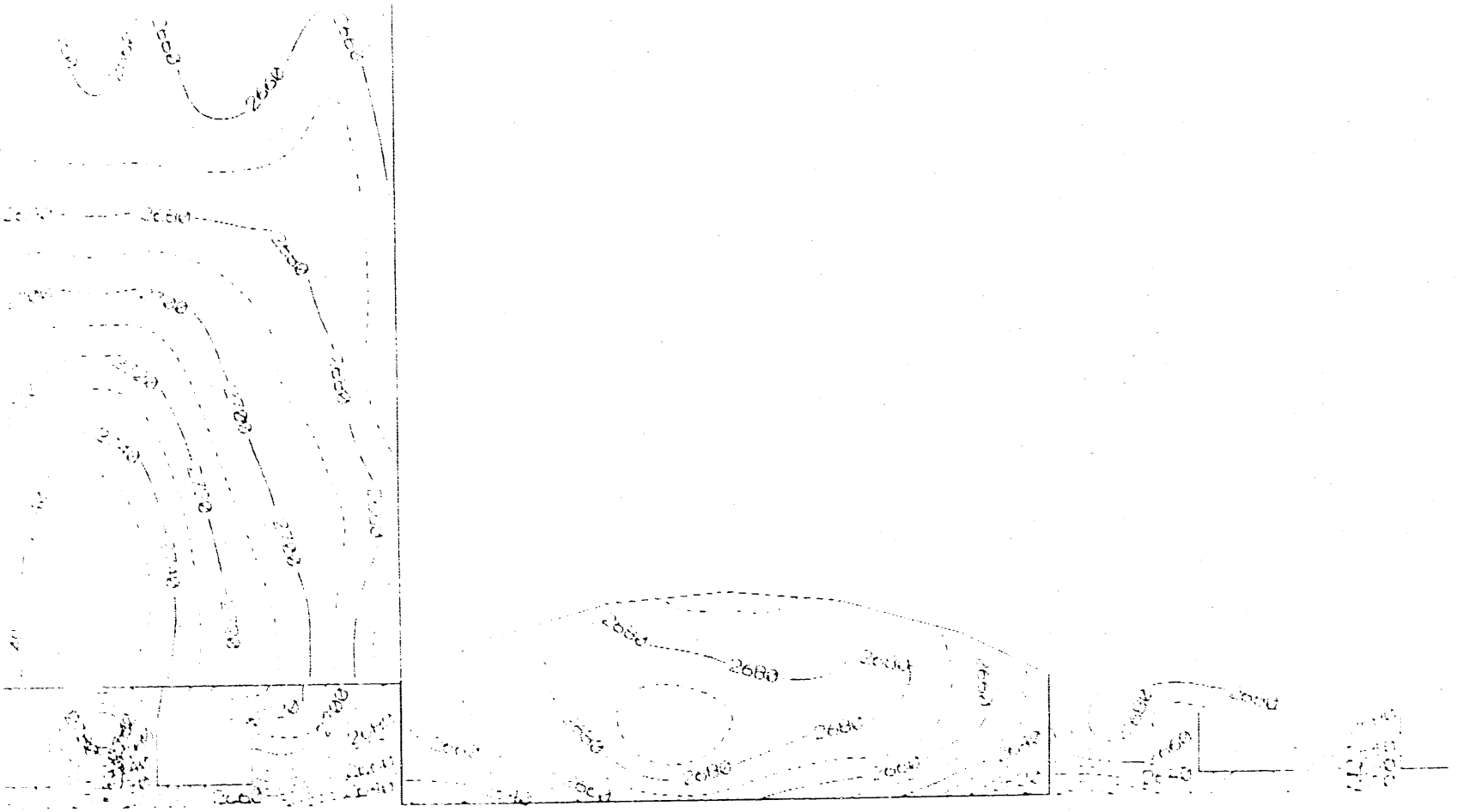

Fig 21

END

DATE FILMED

11 / 30 / 90